BILINGUAL PUBLISHING GROUP

Journal of Environmental & Earth Sciences

https://journals.bilpubgroup.com/index.php/jees

ARTICLE

Assessment of the Solar Energy Potential over South America Estimated by CMIP6 Models in the Present and Future Climate

Glauber W. S. Ferreira**, *Michelle S. Reboita*, *João Gabriel M. Ribeiro

Natural Resources Institute, Federal University of Itajubá, Itajubá, Minas Gerais, 37500–903, Brazil

ABSTRACT

Developing the renewable energy matrix of South America (SA) is fundamental for sustainable socioeconomic growth and mitigating climate change's adverse effects. Thus, this study estimates changes in SA's solar irradiance and solar power potential using data from eight global climate models (GCMs) belonging to the Coupled Model Intercomparison Project—Phase 6 (CMIP6). Applying statistical downscaling and bias correction with the Quantile Delta Mapping (QDM) technique, we evaluate projected changes in the Concentrated Solar Power (CSP) and Photovoltaic Power (PVP) outputs under different future climate scenarios (SSP2-4.5 and SSP5-8.5). Historical simulations (1995–2014) are validated using ERA5 reanalysis and CLARA-A3 satellite observations. The QDM method reduces the models' systematic biases, decreasing the ensemble's errors by 50% across SA throughout the year. Regarding future decades (2020–2099), the CMIP6 ensemble shows spatial and seasonal variability in solar generation. For CSP, estimates suggest that regions traditionally favorable to solar energy generation (such as the Brazilian Northeast and portions of Chile) will maintain their suitable conditions during the 21st century, projecting a potential 1–6% increase (particularly under the SSP5-8.5 scenario in southern Chile and most of Brazil). Concerning PVP generation, the CMIP6 ensemble projects a rise of 1–4% (mainly under the SSP5-8.5 scenario in the Amazonia, Midwest, and Southeast Brazilian sectors). Moreover, trend analyses projected individually by the CMIP6 GCMs converge on an increasing PVP, mainly in Brazil's Amazonia and Midwest regions. In contrast, for South Brazil, approximately 84% of the projections show a negative trend (or no trend), evidencing unfavorable or uncertain conditions for solar generation development in the region. Despite the data and processes' inherent limitations, this study yields a first analysis of statistically downscaled projections from CMIP6 for solar power generation in South America, providing valuable information for energy sector decision-makers.

Keywords: Solar power; CMIP6; Climate change; Statistical downscaling; South America

*CORRESPONDING AUTHOR:

Glauber W. S. Ferreira, Natural Resources Institute, Federal University of Itajubá, Itajubá, Minas Gerais, 37500–903, Brazil; Email: glauber_ferreira@unifei.edu.br

ARTICLE INFO

Received: 25 April 2024 | Revised: 30 May 2024 | Accepted: 13 June 2024 | Published Online: 4 July 2024

DOI: https://doi.org/10.30564/jees.v6i2.6425

CITATION

Ferreira, G.W.S., Reboita, M.S., Ribeiro, J.G.M., 2024. Assessment of the Solar Energy Potential over South America Estimated by CMIP6 Models in the Present and Future Climate. Journal of Environmental & Earth Sciences. 6(2): 110–143. DOI: https://doi.org/10.30564/jees.v6i2.6425

COPYRIGHT

Copyright © 2024 by the author(s). Published by Bilingual Publishing Group. This is an open access article under the Creative Commons Attribution-NonCommercial 4.0 International (CC BY-NC 4.0) License (https://creativecommons.org/licenses/by-nc/4.0/).

1. Introduction

Conciliating socioeconomic growth with sustainable energy development is one of the leading global urgencies. Global warming, intensified by anthropic activities that emit greenhouse gases, has caused surface temperature to rise by approximately 1.1 °C compared to pre-industrial levels [1]. Emissions of greenhouse gases continue to grow, arising from several factors like the use of fossil fuels, land-use change, high consumption patterns etc. [1], and in a more pessimistic scenario, global climate models (GCMs) project an increase in average global temperature of up to 5.7 °C by the end of the 21st century [2]. Indeed, the ten warmest years in historical records have all occurred in the last decade (2014–2023), and 2023 was the warmest year since global recordings began in 1850, being approximately 1.35 °C above the pre-industrial average [3]. In this context, executing decarbonization strategies is crucial to mitigate climate change's negative impacts and meet the Paris Agreement's commitments. For South America (SA), such actions are equally urgent because, despite its leading role worldwide in the use of renewable energies [4], recent years have shown a growing use of non-renewable sources and greenhouse gas emissions [5,6].

Abundant in solar and wind resources, Latin America currently has more than 319 GW of solar and wind energy production capacity (large-scale announced, in pre-construction or under construction) and could increase its production capacity by more than 460% by 2030 compared to the 69 GW (27.6 GW of solar and 41.5 GW of wind) that are currently in operation [7]. In this scenario, Brazil stands out, as the country currently has around 40 GW of installed solar photovoltaic capacity and could reach 68 GW in the next five years, which would place it as the fifth-largest solar producer in the world and the leader in solar production in Latin America [8,9]. However, the expansion of solar capacity in the country depends on several factors, such as the installation of solar farms, the improvement of energy transmission and storage systems, the implementation of a management system that integrates solar energy into the Brazilian matrix, and incentives for new investments in the sector [8].

Solar energy can be generated by two main methods: concentrated solar power (CSP) and photovoltaic solar power (PVP). Concentrated solar power stations collect and concentrate direct sunlight and use it to produce heat and drive a steam turbine to produce electricity. Two CSP technologies stand out: power towers, where flat mirrors focus sunlight on a single point on a high tower, and parabolic troughs, where curved mirrors focus sunlight onto a line running along the mirrors [10]. Most systems use linear concentrating systems via parabolic troughs, whereas power towers are the most widely used point concentrating technology. On the other hand, solar photovoltaic technology uses solar cells to convert solar radiation into electricity directly through the photovoltaic effect [10–12]. They can convert up to 20% of incident solar radiation into electricity, reaching a total installed capacity of 710 GW by the end of 2020 [10,11]. Among the most widely used PVP technologies, crystalline silicon devices account for 80% of the global market, while thin film technology is more recent, offering generally lower costs and more efficiency than crystalline silicon technology [10]. In SA, solar energy has become Brazil's third largest source of electricity, and around 70% of the solar energy produced in the country comes from small crystalline silicon systems installed on the roofs of houses and commercial and rural properties [13].

Several studies have assessed the impacts of climate change on solar radiation and, consequently, on solar energy generation in different parts of the world. Using Coupled Model Intercomparison Project—Phase 3 (CMIP3) models, Crook et al. [14] concluded that, under the A1B scenario, there is a moderate increase (decrease) in PVP generation during the 21st century in Europe and China (the western United States and Saudi Arabia), and significant increases in CSP in the same regions. In addition, dynamically downscaled CMIP3 projections show a reduction of up to 12% in PVP in northern European countries, while southern areas may experience an increase in solar energy generation [15]. Similarly,

CMIP5 model projections indicate favorable conditions for PVP generation in the coming decades in Spain, France, Italy, and Germany [16–20]. In addition to Europe, other regions of the globe also suggest favorable conditions for solar power generation in the future, as projected by CMIP5 models for East Asia, Southeast North America, and Central America [16–20]. Conversely, reduced PVP is projected by CMIP5 and CMIP6 models in Africa, the Middle East, Central Asia, Australia, and North America [18–24].

In general, the increasing PVP generation is associated with a projected decreasing cloud cover [16], so changes in cloud cover and the composition of atmospheric aerosols can affect PVP generation since the electricity produced does not respond linearly to changes in irradiance and depends on the ratio between direct and diffuse radiation [17]. Globally, direct climate impacts on solar energy are expected to be modest (of the order of 5%) because the effects of changes in irradiance are also minor, while the negative impacts of warming occur mainly at higher latitudes, which already have a more limited potential for generating PVP than low latitudes [20].

Regarding SA, it has favorable conditions for solar energy generation, given that the solar resource is evenly distributed on the continent and a large part of it is located in the Region of the Sun Belt with the highest solar radiation, with Chile, Bolivia, and Argentina among the ten countries in the world with the maximum irradiation for PVP systems [25,26]. Some sectors of the continent stand out, such as northern Chile, which has the highest irradiation levels (with the Atacama Desert having the best global maximum irradiation), northeastern Brazil, north of Colombia, the west coast of Peru, and northern Argentina [26]. On the other hand, climate projections from the Coordinated Regional Downscaling Experiment (CORDEX) indicate a reduction of up to 2.49% in the PVP in the central zone of Nariño (far west of Colombia) and a maximum increase of 2.52% in the southeast of the region [27]. Furthermore, solar energy is estimated to supply up to 82% and 86% of electricity generation by 2050 in Bolivia [28] and Chile [29], respectively.

For Brazil, dynamically downscaled climate projections from CMIP5 suggest increased solar radiation over almost the entire country between 2030 and 2080 under the RCP8.5 scenario, resulting in an average increase of 3.6% in PVP in Northeast Brazil by 2080, as well as in locations with installed PVP solar farms in the Northeast and Southeast [30]. In addition, statistically downscaled climate projections from CMIP5 provided three patterns of changes in global horizontal irradiance during the 21st century in Brazil: a pattern of reduction of up to 10% on the north/northeast coast, a reduction of up to 10% in the south of the country in the second half of the year, and a transversal band from the Brazilian Southeast to the Amazonia with an increase of 5 to 10% during the austral summer [31]. On the other hand, raw climate projections from CMIP6 indicate for the 2021–2100 period an increase of up to 5% in CSP in northern Brazil and reductions in the rest of the country of more than 5%, mainly in the Southeast, Midwest, northern portion of the Northeast and portions of the Brazilian North [32]. In contrast, raw climate projections from CMIP5 and CMIP6 suggest growth in energy generated by CSP technology, with a statistically significant average increase of up to 6% in most of Brazil (except the country's southern region) in 2071–2100 [24]. Furthermore, studies show that environmental heating caused by rising temperatures reduces the conversion efficiency of photovoltaic cells [24,32].

GCMs are fundamental tools for evaluating climate elements, but their direct application in studies of regional impacts is inappropriate due to the outputs' coarse resolution. In this sense, statistical and dynamical downscaling techniques are essential for overcoming these limitations of global models. However, their use in studies of climate change's impacts on solar radiation in SA is still embryonic in the literature. Despite helping analyze climate phenomena on a local scale, dynamical downscaling requires high computational costs [33]. On the other hand, statistical downscaling requires fewer computational resources but a long series of local observations [34]. Among the sparse existing studies for the

region, there are analyses obtained by dynamical [30] and statistical downscaling [31], but more current studies with CMIP6 models use their raw outputs [22,24,32]. However, a recent study [35] used the Quantile Delta Mapping (QDM) bias correction method [36] to statistically downscale CMIP6 simulations of irradiation in Brazil, concluding that the technique reduced the systematic biases of the models in both long-term averages and extreme values, demonstrating its potential use for studies of climate impacts in SA.

Given the above, this study aims to: (a) apply QDM bias correction and statistical downscaling to historical simulations and climate projections of solar irradiation from a CMIP6 multi-model ensemble and; (b) use the bias-corrected projections to assess the solar generation potential by CSP and PVP technologies in SA under different greenhouse gas emission scenarios. The relevance of this study is justified by the scarcity of studies on the impacts of climate change on solar energy generation in SA, as well as studies that apply statistical downscaling to CMIP6 solar radiation projections for the continent. In this context, our study fills this gap and seeks to assist policymakers, planners, and decision-makers involved in expanding the solar energy matrix in SA, as well as all those interested in the energy transition on the continent.

2. Materials and methods

2.1 Study area

The study area comprises the South American continent (**Figure 1**), located at 12°N–55°S latitudes and marked by great latitudinal extension, complex topography, and climate heterogeneity with tropical, subtropical, and extratropical regions [37]. SA also has an intricate geography, characterized by disparate areas such as the Andes Mountains, the Atacama Desert, the Amazon Rainforest, and Brazil's semi-arid northeastern region. SA is privileged in terms of solar resources, and a large part of the continent is located in the area of the Sun Belt with the highest solar radiation [25], with some highlighted regions, such as northern Chile, northeastern Brazil, north of Colombia, the west coast of Peru and northern Argentina [26].

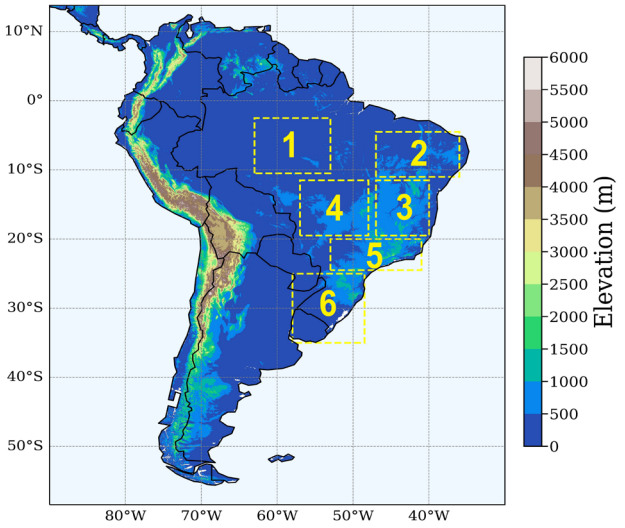


Figure 1. Illustration of the study area with elevation (m). The yellow rectangles indicate subdomains selected for individual analysis of the CMIP6 GCMs.

Source: United States Geological Survey-Earth Resources Observation System (EROS) Center.

2.2 CMIP6 GCMs

This study used surface downwelling shortwave flux, 2 m air temperature, and the zonal and meridional components of wind at 10 m from eight CMIP6 GCMs, covering the historical period (1995–2014) and two greenhouse gas emission scenarios (SSP2-4.5 and SSP5-8.5) for the future period (2020–2099). The GCMs data comprised simulations obtained every three hours provided on the Earth System Grid Federation (ESGF) platform (available at: https://aims2.llnl.gov/search/cmip6/). We employed the Rupp et al. [38] methodology to select the CMIP6 GCMs, whereby various statistical metrics are used to assess the models' performance in simulating a given region's historical climate. Further details on the methodology, including the mathematical formulation and statistical parameters, can be found in Ferreira et al. [39,40] and Reboita et al. [41,42]. However, we emphasize that the choice of models (**Table 1**) considered the GCMs' ability to simulate historical cli-

mate and the availability of high-frequency data and projections on the ESGF platform. Furthermore, of the GCMs selected, three (EC-Earth3, IPSL-CM6A-LR, and MPI-ESM1-2-LR) had already demonstrated a fair ability to represent the South American climate [43]. Moreover, the ensemble composed of the best-performing models produces results closer to the observations and surpasses the quality of the individual GCM simulations [43].

2.3 Reference data

To validate the climate simulations of the CMIP6 GCMs, we used the ERA5 reanalysis product [52] from the European Centre for Medium-Range Weather Forecasts—ERA5 (ECMWF-ERA5). The variables used were surface solar irradiance (surface downwelling shortwave flux), 2 m air temperature, zonal and meridional wind components at 10 m height, available at a temporal frequency of three hours and with a horizontal resolution of 0.25° for the 1995–2014 reference period (available at: https://cds.climate.copernicus.eu/). Although the ERA5 reanalysis product is an advanced dataset generated by assimilating observations and numerical simulations, it still has systematic biases [21,53,54].

Therefore, to complement the validation data set and overcome the limitations of the reanalysis product, we used satellite observations provided by CLARA-A3, which is a set of cloud, albedo, and surface radiation climate records generated by the Satellite Application Facility on Climate Monitoring (CM SAF), belonging to the European Organization for the Exploitation of Meteorological Satellites (EUMETSAT). CLARA-A3 is the third edition of the CLARA (CM SAF Cloud, albedo, and surface radiation) product, which provides information on cloud properties and radiation parameters derived from the Advanced Very High Resolution Radiometer (AVHRR) sensor, on board the polar-orbiting satellites of the National Oceanic and Atmosphere Administration (NOAA) and Meteorological Operational Satellite Programme (EUMETSAT Metop) [55]. The CLARA-A3 data was obtained from the CM SAF platform, with a horizontal resolution of 0.25º and a daily frequency for the period 1995–2014 (available at https://www.cmsaf.eu/EN/Home/home_node.html). In general, satellite-based observations have fewer uncertainties than reanalysis data due to their greater accuracy [21,56] and are widely used to evaluate solar irradiance simulated by climate models [21].

Table 1. Information on each CMIP6-GCM employed in the study.

Model	Resolution (Lat × Lon)	Institute	Reference
CMCC-CM2-SR5	1.25 × 0.94	Fondazione Centro Euro-Mediterraneo sui Cambiamenti Climatici	Lovato and Peano [44]
CMCC-ESM2	1.25 × 0.94	Fondazione Centro Euro-Mediterraneo sui Cambiamenti Climatici	Lovato et al. [45]
EC-Earth3	0.70 × 0.70	EC-Earth Consortium	Döscher et al. [46]
GFDL-ESM4	1.25 × 1.00	Geophysical Fluid Dynamics Laboratory	Krasting et al. [47]
IPSL-CM6A-LR	2.50 × 1.26	Institut Pierre Simon Laplace	Boucher et al. [48]
MIROC6	1.41 × 1.41	Japan Agency for Marine-Earth Science and Technology	Tatebe and Watanabe [49]
MPI-ESM1-2-LR	0.94 × 0.94	Max Planck Institute for Meteorology	Wieners et al. [50]
MRI-ESM2-0	1.13 × 1.13	Meteorological Research Institute	Yukimoto et al. [51]

2.4 Bias Correction and Statistical Downscaling (BCSD)

Due to their coarse resolution, the raw output of GCMs is unsuitable for use in different applications, such as synoptic scale studies. Given this, we applied statistical downscaling to the CMIP6 outputs (2 m air temperature and zonal and meridional wind components) using the ERA5 reanalysis as a reference set. For the solar irradiance variable, we used the

ensemble mean of CLARA-A3 observations and the ERA5 reanalysis to apply the advantages obtained by both sets. Among the different categories of statistical downscaling methods (transfer or regression models, weather generator, weather typing), we applied the transfer function, which establishes statistical relationships between the observed and modeled variables [57]. This methodology is also called Bias Correction—Statistical Downscaling (BCSD). Before BCSD, spatial disaggregation was applied to the CMIP6 outputs so that all the data from the models, the ERA5 reanalysis, and the CLARA-A3 observations were interpolated to a resolution of 0.5° × 0.5° using bilinear interpolation since studies have shown the ability of this method to generate consistent fields [35,58].

For the BCSD method, we used the QDM technique [36] for historical simulations (1995–2014) and applied transfer functions to future projections (2015–2099) of each CMIP6 model. The QDM technique is justifiable for statistical downscaling because it preserves the relative changes and trends projected by the models and corrects systematic biases in the modeled data's quantiles concerning the observations' distribution [36]. In general, the QDM process follows three stages: first, the trend is removed from all simulated and projected quantiles individually; then, the bias is corrected using the quantile mapping technique for all quantiles with the trend removed; and finally, the projected changes are superimposed on the bias-corrected outputs [36]. The reader can find more details on the BCSD methodology in Ferreira et al. [39,40] and Reboita et al. [41,42].

The historical period (1995–2014) composed the training set to adjust the future projections (2015–2099) with the QDM algorithm to optimize computational resources and follows the same reference period used by the International Panel on Climate Change—IPCC [59]. The Python-based package xclim [60] was used to perform the calculations. According to Cannon et al. [36], the QDM technique is advantageous over quantile mapping because it is less susceptible to the inflating relative trends in extreme values, which was demonstrated in a recent study using the method to downscale different atmospheric variables simulated by CMIP6 for SA [35].

2.5 Solar energy

CSP and PVP technologies are the most widely used for generating solar energy [10–12,24]. CSP systems produce electricity with the thermal energy of sunlight through a process whereby the light is concentrated on a receiver using various mirrors or lenses and is then used to produce heat that drives the engine and electricity generator [24]. On the other hand, the PVP system converts sunlight directly into electricity through PVP panels using semiconductor materials, which absorb light and generate electricity through the photovoltaic effect [12,24]. As reported by Ha et al. [24], the empirical equations and coefficients used here evaluate the solar energy potential as a function of different atmospheric variables and how changes in climate conditions resulting from global warming can influence this potential, not considering technological advances that may alter future solar energy generation.

Concentrated Solar Power (CSP)

CSP technology can be classified into four different categories based on the type of collector: parabolic trough collector (PTC), solar power tower (SPT), linear Fresnel reflector, and parabolic dish collector [24]. In this study, the equations and coefficients used refer to the PTC system since this technology is the most mature and globally consolidated among the technologies for concentrating solar energy, both commercially and on an industrial scale [61–64], as well as being the most widespread technology in plants for thermoelectric generation from solar energy in Brazil [65].

Here, we apply the methodology proposed by Crook et al. [14], which is consolidated in the literature with various studies [20–22,24,32], whereby the CSP output (CSP_{out}) is estimated using the thermal efficiency of CSP (η_{CSP}) multiplied by the direct irradiance (R_d), see equation (1):

$$CSP_{out} = \eta_{CSP} \times R_d \quad (1)$$

η_{CSP} is expressed as a function of surface air temperature (TAS) and R_d, see equation (2):

$$\eta_{CSP} = k_0 - k_1 \times \frac{(T_i - TAS)}{R_d} \quad (2)$$

The specific collector coefficients $k_0 = 0.762 Wm^{-2}℃^{-1}$, $k_1 = 0.2125 Wm^{-2}℃^{-1}$ and fluid temperature $T_i = 115℃$ were tested on the Industrial Solar Technology parabolic trough collector at Sandia National Laboratories [21,24] and applied in several studies [14,20–22,24,32].

As R_d is not provided directly by the CMIP6 models, it is necessary to derive it from an empirical relationship between fractional cloud cover (fclt) and clear sky irradiance at the surface (R_{sc}) [21,24], see equation (3):

$$R_d = 0.75 \times R_{sc} \times (1 - fclt) \quad (3)$$

where the factor 0.75 represents the scattering effect of sunlight by air molecules and aerosols [21]. As R_{sc} is also not provided by the CMIP6 GCMs, the relationship between fclt, solar irradiance at the surface (R_s) and R_{sc} is used as follows [21,24], see equation (4):

$$fclt = 1 - \frac{R_s}{R_{sc}} \quad (4)$$

By grouping equations 3 and 4, it is possible to estimate R_d using equation (5):

$$R_d = 0.75 \times R_s \quad (5)$$

Photovoltaic Power Potential (PVP_{pot})

Following the methodology widely used in the literature [15,16,18-24,32], we estimated the photovoltaic power potential (PVP_{pot}) utilizing the energy rating method, which multiplies the total integrated solar irradiance over a period by a performance ratio [24] through the expression, see equation (6):

$$PVP_{pot} = P_R \times \frac{Rs}{Rs_{STC}} \quad (6)$$

where STC refers to the standard test conditions ($Rs_{STC} = 1000 Wm^{-2}$), under which the nominal capacity of a photovoltaic device is determined, and P_R is the performance ratio that accounts for changes in the efficiency of photovoltaic cells due to temperature changes, according to equation (7) [24]:

$$P_R = 1 + \gamma \times [T_{cell} - T_{STC}] \quad (7)$$

where T_{STC} is the ambient air temperature under standard test conditions ($T_{STC} = 25℃$), γ is -0.005 $℃^{-1}$, following the typical response of monocrystalline silicon solar panels adopted in different studies [15,20,21,24]. Here, we consider the generation of solar energy by monocrystalline silicon solar panels since these (together with polycrystalline silicon solar panels) account for up to 80% of the global photovoltaic energy market [66], as well as being widely used in SA, given that around 70% of the solar energy produced in Brazil comes from small crystalline silicon systems installed on the roofs of houses and commercial and rural properties [13]. T_{cell} is the temperature of the photovoltaic cell, which is affected by Rs, TAS, and wind speed (WS, calculated with the zonal and meridional components of the wind). Although some studies [21,24] have shown that the contribution of wind speed is practically negligible for changes in PVP_{pot}, here we have chosen to include the variable in the estimate of photovoltaic energy generation using equation 8, widely adopted in the literature [15,16,18–24,32]:

$$T_{cell} = c_1 + c_2 \times TAS + c_3 \times Rs + c_4 \times WS \quad (8)$$

where $c_1 = 3.9℃$, $c_2 = 0.942$, $c_3 = 0.028℃\ m^{-2}W^{-1}$, and $c_4 = -1.509℃\ sm^{-1}$. For better analysis, the value of PVP_{pot} is multiplied by 100 and is therefore referred to in %.

PVP_{pot} Anomalies and trend time series

Additionally, only for the SSP5-8.5 scenario, we present the trend and change projections estimated by each CMIP6 GCM (as well as by the multi-model ensemble) for 2020–2099 concerning the 1995–2014 period for six key regions (**Figure 1**) that concentrate solar energy hotspots in SA [67]: Brazilian Amazonia (R1; 2.5°S–10°S, 53°W–63°W), northern sector of the Brazilian Northeast (R2; 4.5°S–11°S, 36°W–47°W), southern and central sectors of the Brazilian Northeast (R3; 11°S–19.5°S, 40°W–47°W), the Brazilian Midwest (R4; 11.5°S–19.5°S, 48°W–57°W), the Brazilian Southeast (R5;

20°S–24.5°S, 41°W–53°W), and the Brazilian South and Uruguay (R6; 25°S–35°S, 48.5°W–58°W). This analysis assesses the temporal evolution of the spread among the different CMIP6 models' projections.

Test of statistical significance for the difference in mean climatological values and Mann-Kendall Trend Test

We used the Student's *t*-test to assess whether the differences in the mean seasonal climatological values of CSP and PVP for the future period (2020–2099) projected by the CMIP6 ensemble are statistically significant about the historical period (1995–2014), using an α significance level of 5%. Furthermore, under the SSP5-8.5 scenario, we analyzed the trend time series of PVP obtained by the eight CMIP6 models and the multi-model ensemble for six SA subdomains (**Figure 1**) to present the climate change signal in different solar hotspot sectors [67]. This procedure was carried out using the Mann-Kendall test, widely used to analyze trends in climate series [68]. In addition, Sen's slope estimation test was used to detect the linear trend of PVP_{pot} in the subdomains evaluated.

3. Results and discussion

Historical simulations

Figure 2 shows the historical seasonal climatology (1995–2014) of surface downwelling shortwave radiation (W m^{-2}) provided by the outputs of the four datasets used: the ERA5 reanalysis, the CLARA-A3 satellite observations, the simulations obtained by the ensemble composed of CLARA-A3+ERA5 and, finally, the original (pre-processed) historical simulations of the CMIP6 ensemble. The biases of the four datasets are also presented: the bias of CMIP6 statistically downscaled with the ERA5 reanalysis; the bias of CMIP6 statistically downscaled with the CLARA-A3 satellite observations; the bias of CMIP6 statistically downscaled with the CLARA-A3 + ERA5 ensemble; and bias of the original CMIP6 ensemble simulations in relation to the CLARA-A3 + ERA5 ensemble. In general, all the ensembles show their systematic biases, with a predominance of underestimates of up to 20 W m^{-2} in much of central Brazil and northeastern Brazil and overestimates of the same magnitude in Argentina, Chile, and northern SA during the DJF months. Similarly, in the months of MAM and JJA, overestimates of up to 20 W m^{-2} prevail over most of the continent, including Argentina, Chile, the southern and northern sectors of Brazil, and northern SA. For the months of SON, there is a significant reduction in bias across the continent despite a persistent positive bias of up to 20 W m^{-2} in northeast Brazil's coastal and central regions. Nevertheless, the CMIP6 downscaled simulations with the CLARA-A3 + ERA5 ensemble provide biases between –10 and 10 W m^{-2} over most of SA (except in JJA).

Figure 3 illustrates the satisfactory performance of statistical downscaling with the CLARA-A3 + ERA5 ensemble, which shows the seasonal climatology of solar irradiance and biases (in percentages). The reduction in systematic errors by the BCSD technique with the CLARA-A3 + ERA5 ensemble is notable, indicating a decrease of up to 50% in the magnitude of the biases over most of the continent. For almost the entire year, the biases are between -5 and 5%, with the months of JJA showing more systematic errors in Brazil's central-southern and northeastern sectors, Paraguay, central-southern Peru, Suriname, and the Guianas. In addition, a positive (negative) bias of up to 10% persists in the months of JJA and SON (DJF and MAM) in northeastern Brazil. However, this Brazilian region is one of the global sectors where CLARA-A3 does not satisfactorily achieve its accuracy objective [55].

The CSP_{out} results (**Figure 4**) show that the highest seasonal values of CSP in SA also occur in spring due to the higher magnitudes of solar irradiance at the surface at this time of year. During this season, the highest magnitudes of concentrated solar energy occur in northeastern Brazil and the west coast of SA, where concentrated energy exceeds 160 W m^{-2}. In other regions of Brazil, such as the center-southeast of the country, the values are between 140 and 160 W m^{-2}. In addition, the concentrated energy reaches up to 140 W m^{-2} in the Amazonia region. In the fall and winter seasons, CSP is reduced across the continent, and the west coast of SA and the northern part of the Brazilian Northeast concentrate higher intensities, where values reach up to 180 W m^{-2}.

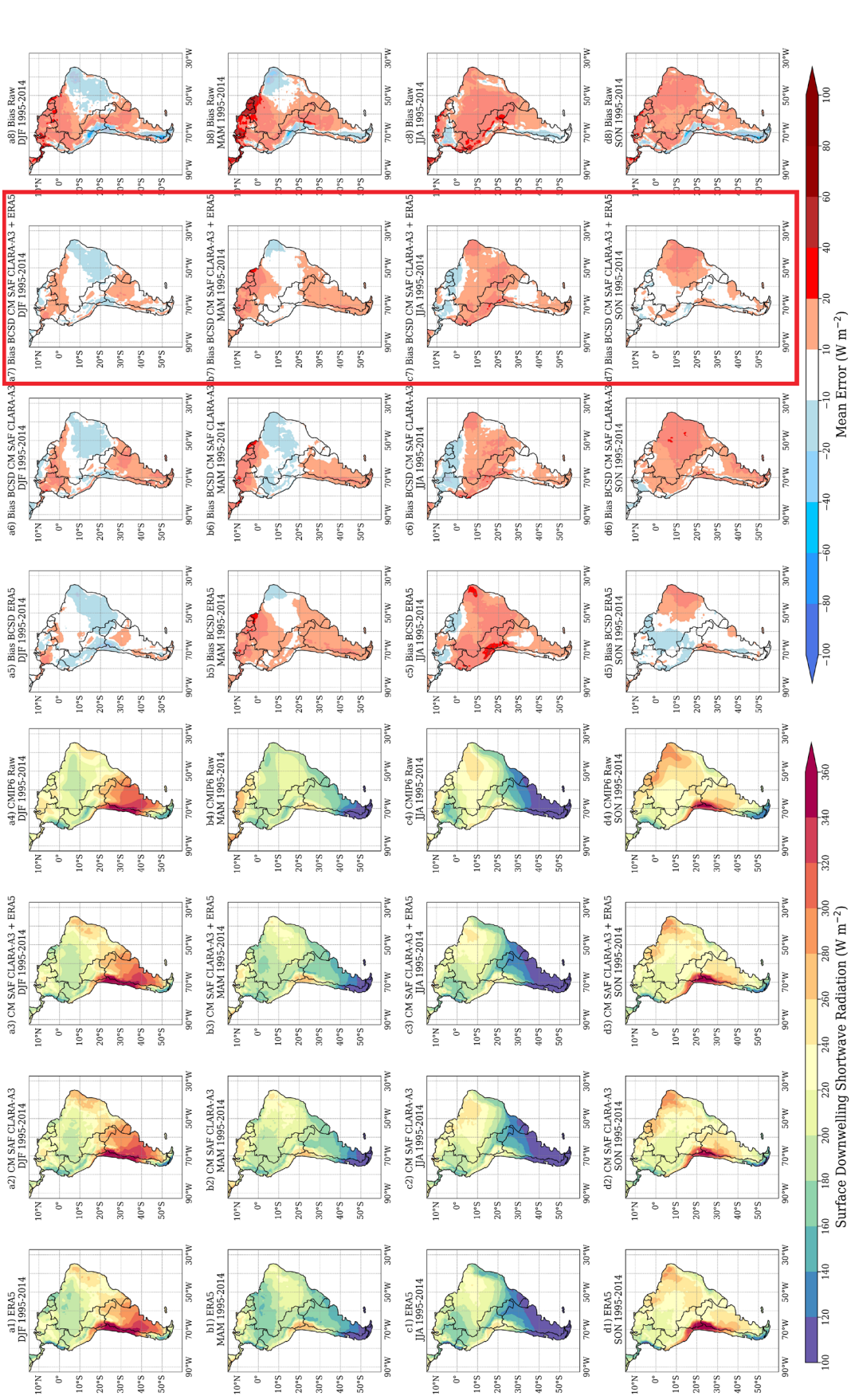


Figure 2. Seasonal climatology of surface downwelling shortwave radiation (W m^{-2}) over the historical period (1995–2014) obtained by ERA5 (first column on the left); CLARA-A3 satellite observations (second column on the left); CLARA-A3 + ERA5 ensemble mean (third column on the left); original CMIP6 ensemble simulations (fourth column on the left). Seasonal climatology of bias (W m^{-2}) in the historical period (1995–2014) between CMIP6-ERA5 statistically downscaled and ERA5 (fourth column from the right); CMIP6-CLARA-A3 statistically downscaled and CLARA-A3 (third column from the right); CMIP6-CLARA-A3 + ERA5 statistically downscaled and CLARA-A3 + ERA5 ensemble (second column from the right); original CMIP6 ensemble simulations and CLARA-A3 + ERA5 ensemble (first column from the right). The red rectangle highlights the ensemble's bias (CMIP6-CLARA-A3 + ERA5 statistically downscaled) selected to analyze the solar power projections.

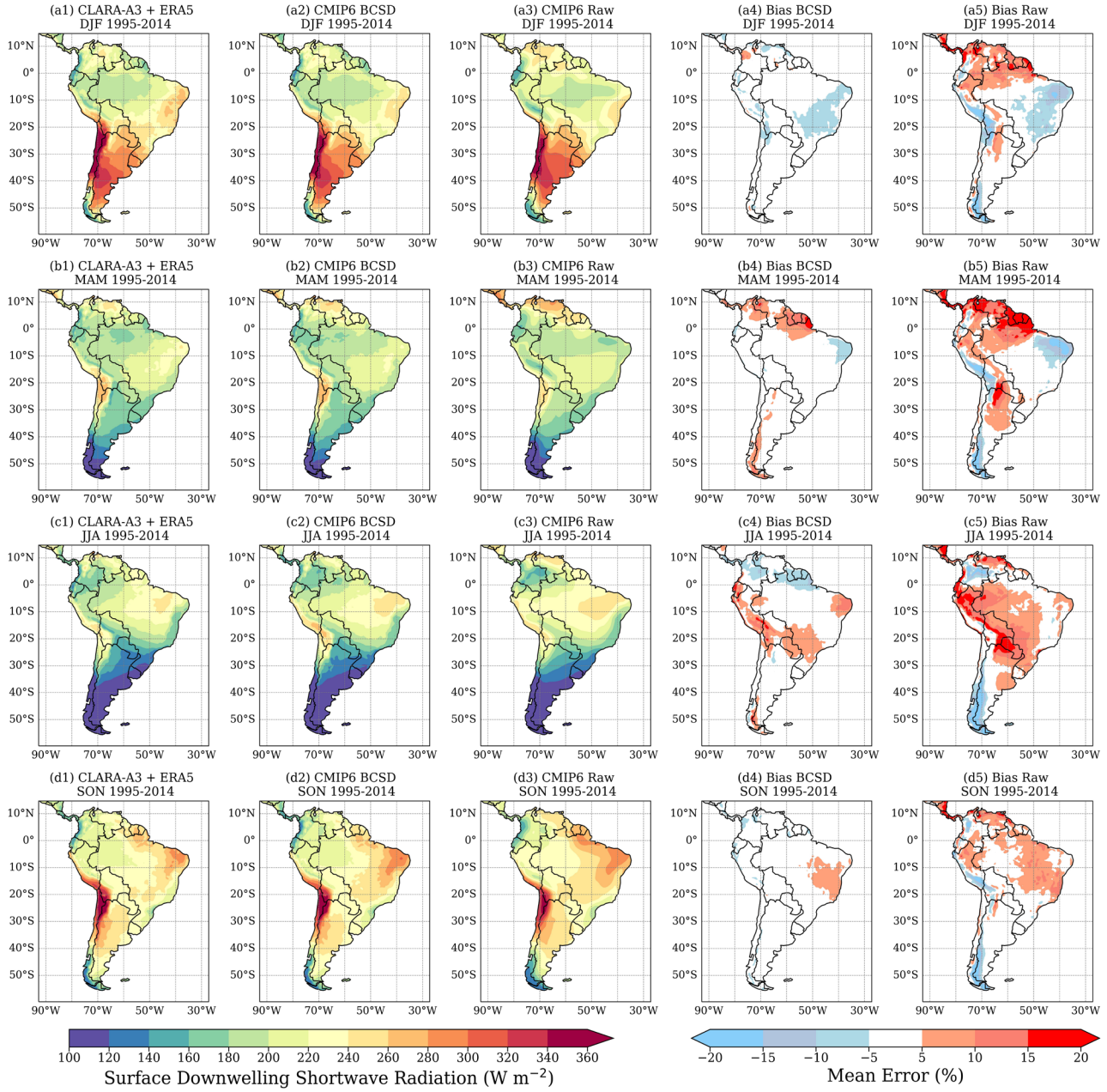


Figure 3. Seasonal climatology of surface downwelling shortwave radiation (W m^{-2}) in the historical period (1995–2014) obtained by the CLARA-A3 + ERA5 ensemble (first column on the left), CMIP6-CLARA-A3 + ERA5 statistically downscaled (second column on the left), original CMIP6 ensemble simulations (middle column); and seasonal bias (%) between the CMIP6-CLARA-A3 + ERA5 statistically downscaled and the CLARA-A3 + ERA5 ensemble (second column from the right), and between the original CMIP6 ensemble's simulations and the CLARA-A3 + ERA5 ensemble (first column from the right).

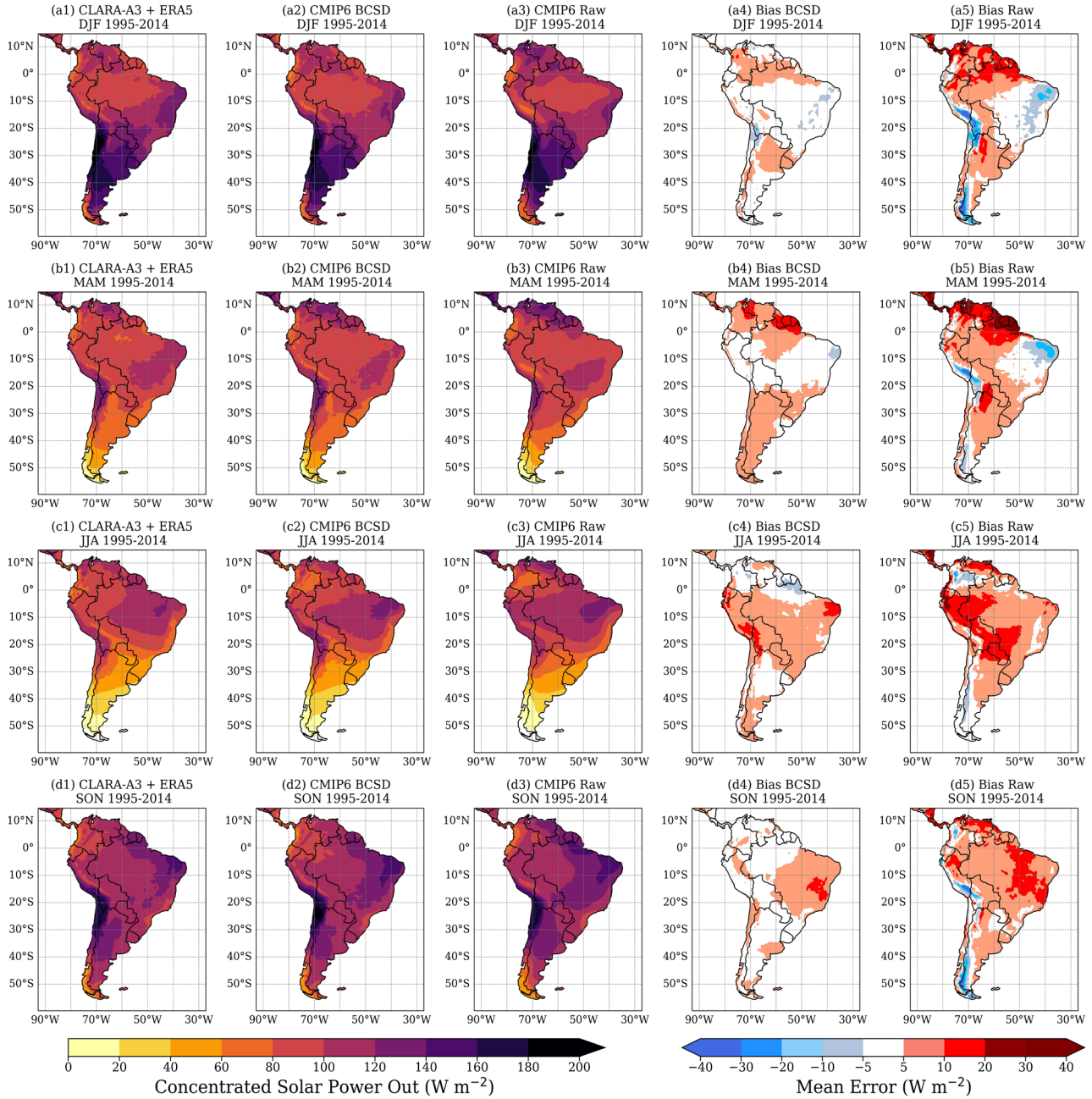


Figure 4. Seasonal climatology of CSP_{out} (W m^{-2}) in the historical period (1995–2014) obtained by the CLARA-A3 + ERA5 ensemble (first column on the left), CMIP6-CLARA-A3 + ERA5 statistically downscaled (second column on the left), original CMIP6 ensemble simulations (middle column) and seasonal bias (W m^{-2}) between the CMIP6-CLARA-A3 + ERA5 statistically downscaled and the CLARA-A3 + ERA5 ensemble (second column on the right) and original CMIP6 ensemble's simulations and the CLARA-A3 + ERA5 ensemble (first column on the right).

The bias fields show that the CMIP6 ensemble tends to overestimate CSP over practically the whole of SA, with positive biases of up to 20 W m^{-2} north of 20°S throughout the year. Additionally, underestimates of up to 20 W m^{-2} occur in the northern sector of the Brazilian Northeast during the first half of the year. Furthermore, underestimates of up to 30 W m^{-2} occur on the west coast of SA throughout the year. The BCSD technique significantly reduces the GCMs' systematic errors, especially in the austral spring and summer. After applying BCSD during the summer, the ensemble biases are between –5 and 5 W m^{-2} over practically the entire continent. However, underestimates (overestimates) of up to 10 W m^{-2} (–10 W m^{-2}) remain in the Northeast region during the summer (spring). In the fall and winter seasons, the prevalence of CSP overestimates remains throughout the continent despite BCSD reducing errors, especially in the Amazonia region and northern SA.

The PVP_{pot} results (**Figure 5**) indicate spatial fields similar to CSP_{out}'s. The highest PVP occurs during spring and regions such as the Brazilian Northeast and the west coast of SA show values of up to 36%. In other areas of Brazil, the values are between 20 and 28% for most of the year. Similarly to the CSP bias fields, the CMIP6 raw ensemble shows systematic overestimates in northern Brazil and northern SA, with a positive bias of up to 6%. Conversely, underestimates of up to 4% occur in northeastern Brazil during the summer and fall, while the Andean region shows underestimates of up to 6%. The BCSD technique considerably reduces the systematic errors of the models, especially in the spring and summer months, when biases of between –1 and 1% are found in practically all of SA. On the other hand, positive biases of up to 2% predominate on the continent in the fall and winter months.

CSP_{out} and PVP_{pot} projections

Figures 6 and **7** show the seasonal difference (in percent) in CSP_{out} after applying statistical downscaling with the CLARA-A3 + ERA5 ensemble under the SSP2-4.5 and SSP5-8.5 scenarios, respectively. The seasonal differences refer to the changes in the 2020–2039, 2040–2059, 2060–2079, and 2080–2099 periods compared to the 1995–2014 historical period. For the DJF months, the projections indicate statistically significant increases in CSP of up to 4% in Brazil's southern and northern regions by 2059 under the SSP2-4.5 scenario. Under the SSP5-8.5 scenario, there is a statistically significant increase of over 3% in the Brazilian Amazonia from 2040 onwards. From 2060 onwards, the SSP2-4.5 scenario projects increased CSP by up to 4% in almost all Brazil. On the other hand, the SSP5-8.5 scenario projects more intense increases (above 4%) for summer from 2060 onwards in a large part of the northern region of Brazil, Peru, Ecuador, southern Colombia, Venezuela, Suriname, and the Guianas, and reductions of up to 2% in the northern part of the Brazilian Northeast.

For the MAM months, the SSP2-4.5 scenario shows no statistically significant increase until 2059, while the SSP5-8.5 scenario indicates increases of up to 4% in northwestern SA. From 2060 onwards, both scenarios show increases of over 3% in the Amazonia region and a reduction of the same intensity in north-central Argentina.

Considering the months of JJA, both scenarios indicate a statistically significant increase of up to 2% in areas of the north and northeast of Brazil by 2059. From 2060 onwards, both scenarios maintain their projections of a significant increase of over 3% in Brazil's Southeast, Northeast, and North regions, with a more intense signal under the SSP5-8.5 scenario.

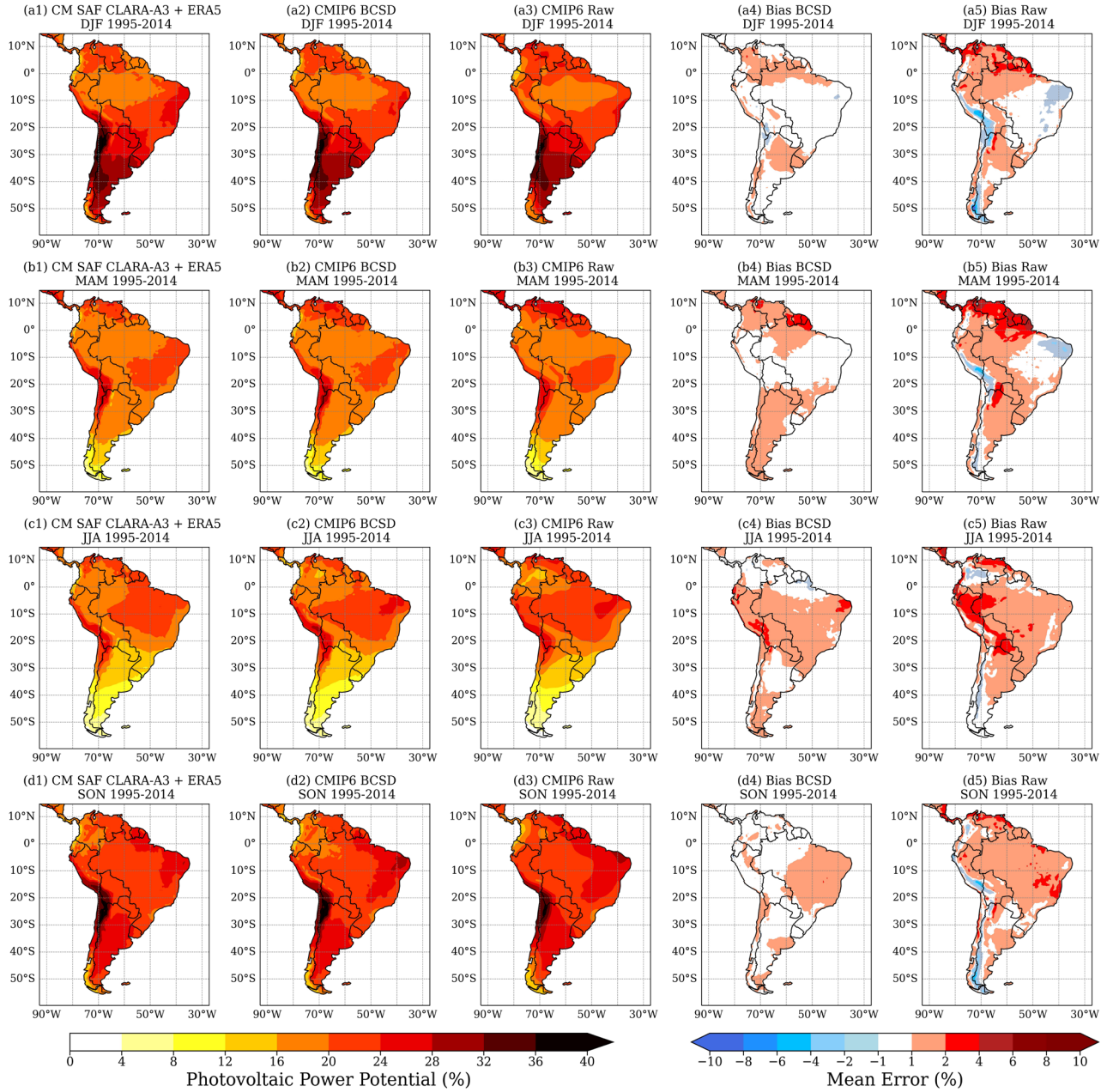


Figure 5. Seasonal climatology of PVP_{pot} (%) in the historical period (1995–2014) obtained by the CLARA-A3 + ERA5 ensemble (first column on the left), CMIP6-CLARA-A3 + ERA5 statistical downscaling (second column on the left), original CMIP6 ensemble simulations (middle column) and seasonal bias (%) between the CMIP6-CLARA-A3 + ERA5 statistical downscaling and the CLARA-A3 + ERA5 ensemble (second column on the right) and original CMIP6 ensemble's simulations and the CLARA-A3+ERA5 ensemble (first column on the right).

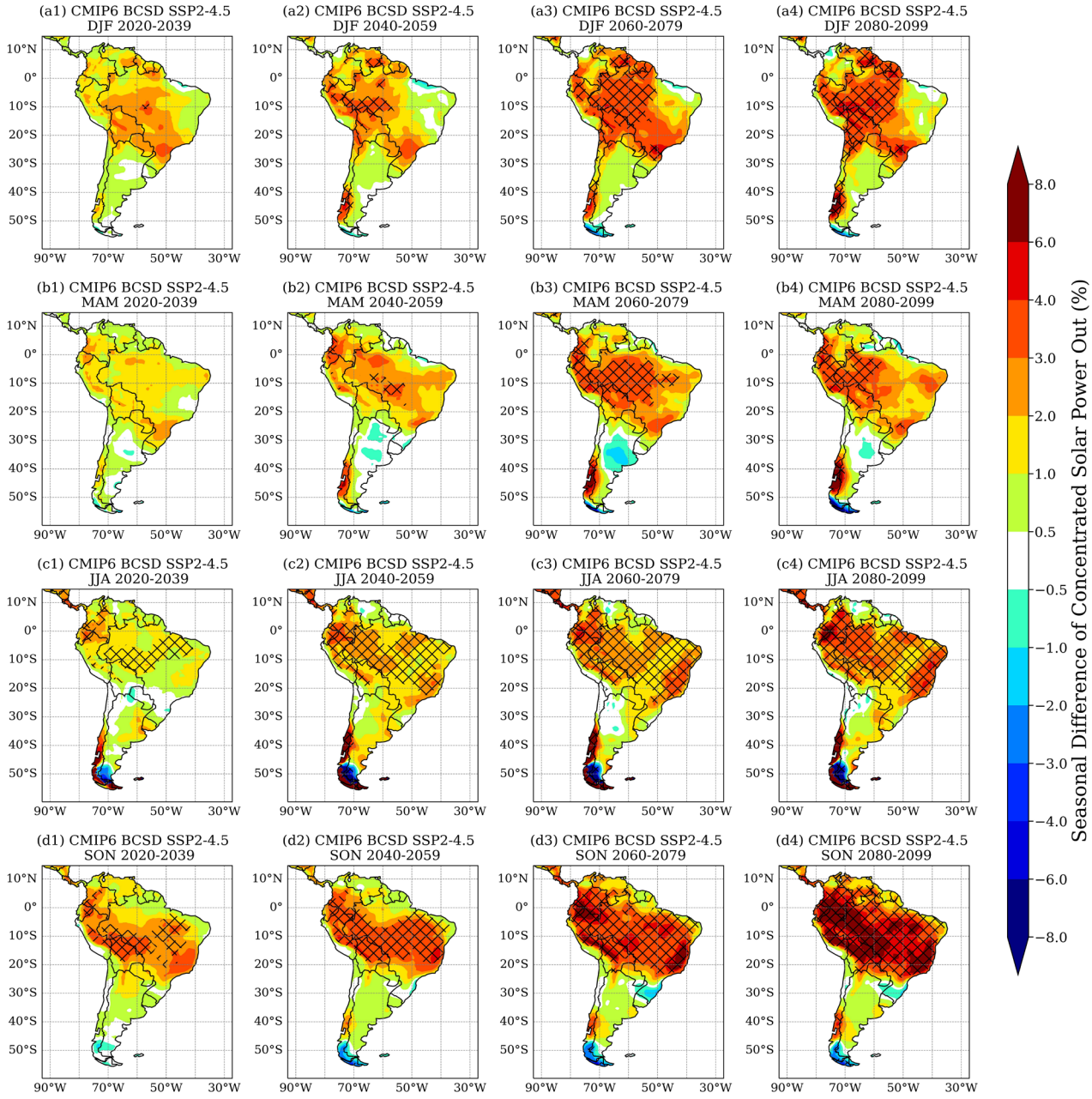


Figure 6. Seasonal difference (%) in CSP_{out} projected by the CMIP6 ensemble after BCSD with the CLARA-A3 + ERA5 ensemble under the SSP2-4.5 emission scenario for the periods 2020–2039, 2040–2059, 2060–2079, and 2080–2099 in relation to the historical period (1995–2014). Hatched areas indicate a statistical significance of 95%, based on the Student's *t*-test.

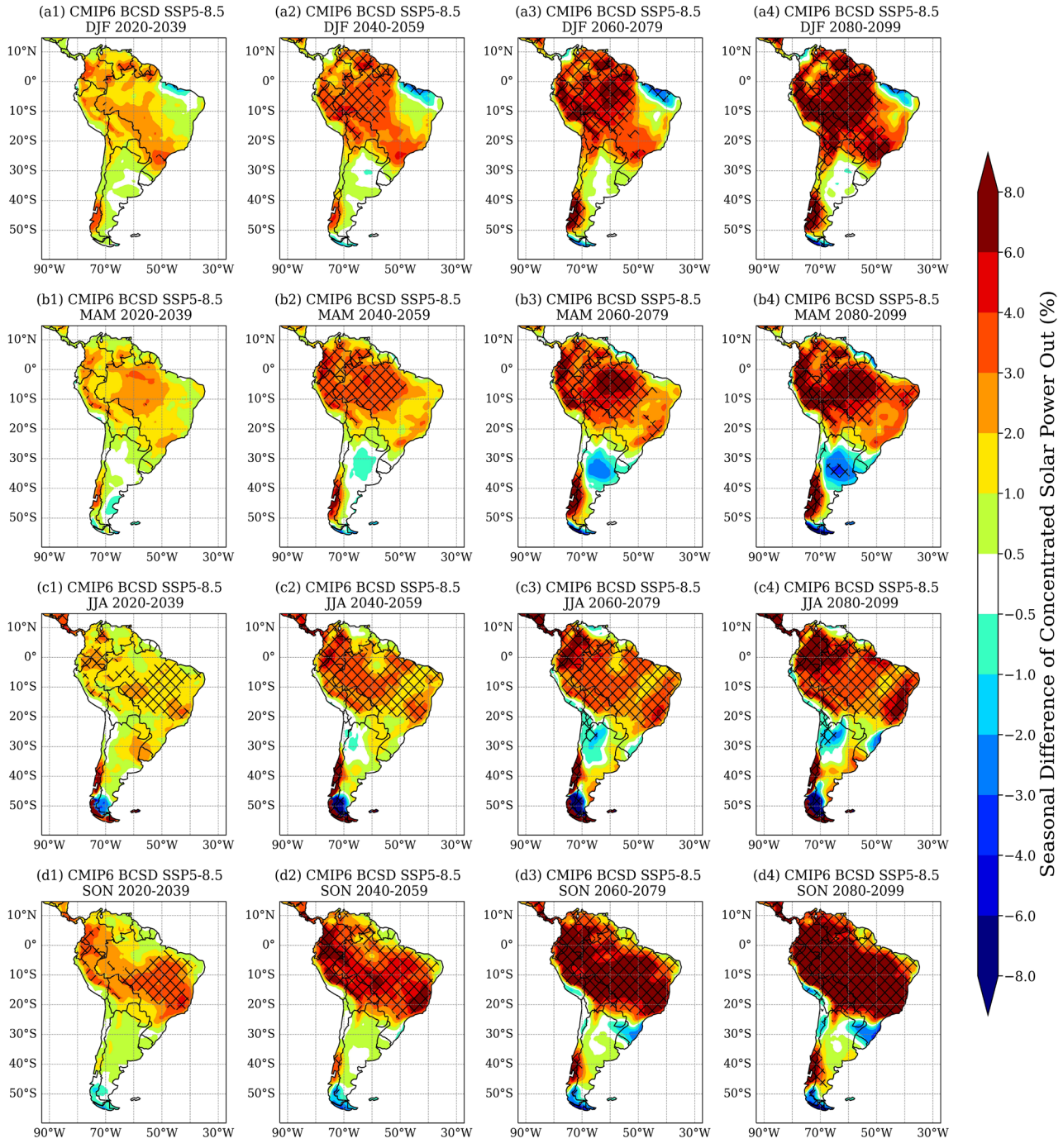


Figure 7. Similar to **Figure 6**, except for the SSP5-8.5 scenario.

About SON months, both scenarios show a significant increase of over 3% in the Southeast, Northeast, and North regions by 2059, as well as in Peru, Bolivia, Ecuador, and Colombia. From 2060 onwards, the two scenarios suggest an intensified increase in almost all of Brazil (as well as the other countries mentioned and Venezuela) and a reduction in the extreme south of Chile and Rio Grande do Sul (Brazil). In general, CSP projections suggest a favorable scenario for solar power generation in SA, mainly in sectors of Brazil such as the Southeast, Midwest, and Northeast coast (depending on the season and emission scenario), Bolivia, Peru, Ecuador, Colombia, and Venezuela. At the same time, reductions are estimated for the southern region of Brazil. These results corroborate projections of concentrated solar energy provided by CMIP3 models for the second half of the 21st century [14].

Figures 8 and **9** show the seasonal difference (in percentage) in PVP_{pot} under the SSP2-4.5 and SSP5-8.5 scenarios, respectively. To the DJF months of the 2020–2059 period, both scenarios project an increase of up to 2% in the Brazilian Amazonia and northern Peru, a pattern also obtained by an ensemble made up of five CMIP6 GCMs under the same scenarios for the DJF months of the 2015–2040 period [22], as well as by an ensemble of seven CMIP5 GCMs under the RCP-4.5 scenario for the summer of 2036-2065 [19].

From 2060 onwards, both scenarios maintain their trend of a significant increase of more than 1% in a large part of the Midwest and North regions and portions of the Brazilian Southeast, as well as Bolivia, Peru, Ecuador and Venezuela. The SSP5-8.5 scenario projects a more intense sign of change, indicating a significant increase of over 3% in practically all of northwestern SA from 2080 onwards. Similarly, ensemble projections of five CMIP6 GCMs indicate an increase of approximately 6% in PVP at latitudes above 20ºS under the SSP1-2.6, SSP2-4.5, and SSP5-8.5 scenarios for the period 2041–2100 [22]. In addition, there are up to 2% reductions in the northern sector of northeastern Brazil, southern Brazil, Uruguay, and south-central Argentina, previously obtained with CMIP6 projections [24,32].

For the MAM months, the projected changes are more modest during the 2020–2059 period, with both scenarios indicating non-significant increases of up to 2%. For the decades from 2060 onwards, the scenarios reinforce the pattern of change, with the SSP5-8.5 scenario extending the areas with an increase of more than 2% to the Brazilian Northeast from 2080 onwards, and extending the core of maximum increase in central Amazonia, as well as a reduction of the same magnitude in central Argentina. These results corroborate CMIP6 projections previously analyzed for the austral autumn of 2015–2100 [22].

Considering the months of JJA, the scenarios show significant increases of up to 1% in most of Brazil, Peru, and Colombia by 2059, with more evident increases projected by the SSP5-8.5 scenario. These results reiterate those of Dutta et al. [22], which found an increase of up to 4% in photovoltaic energy potential in Brazil during JJA of 2015–2040. For the decades from 2060 onwards, the increases persist in the areas already mentioned, including significant increases of over 2% in the Brazilian Southeast and Northeast coastal areas, projected by both scenarios. Similarly, these areas also showed a rise of over 2% in the austral winter of 2041–2100 under the SSP1-2.6, SSP2-4.5, and SSP5-8.5 scenarios [22]. Furthermore, reductions of up to 3% persist in central-southern Brazil, central-northern Argentina, and the west coast of SA.

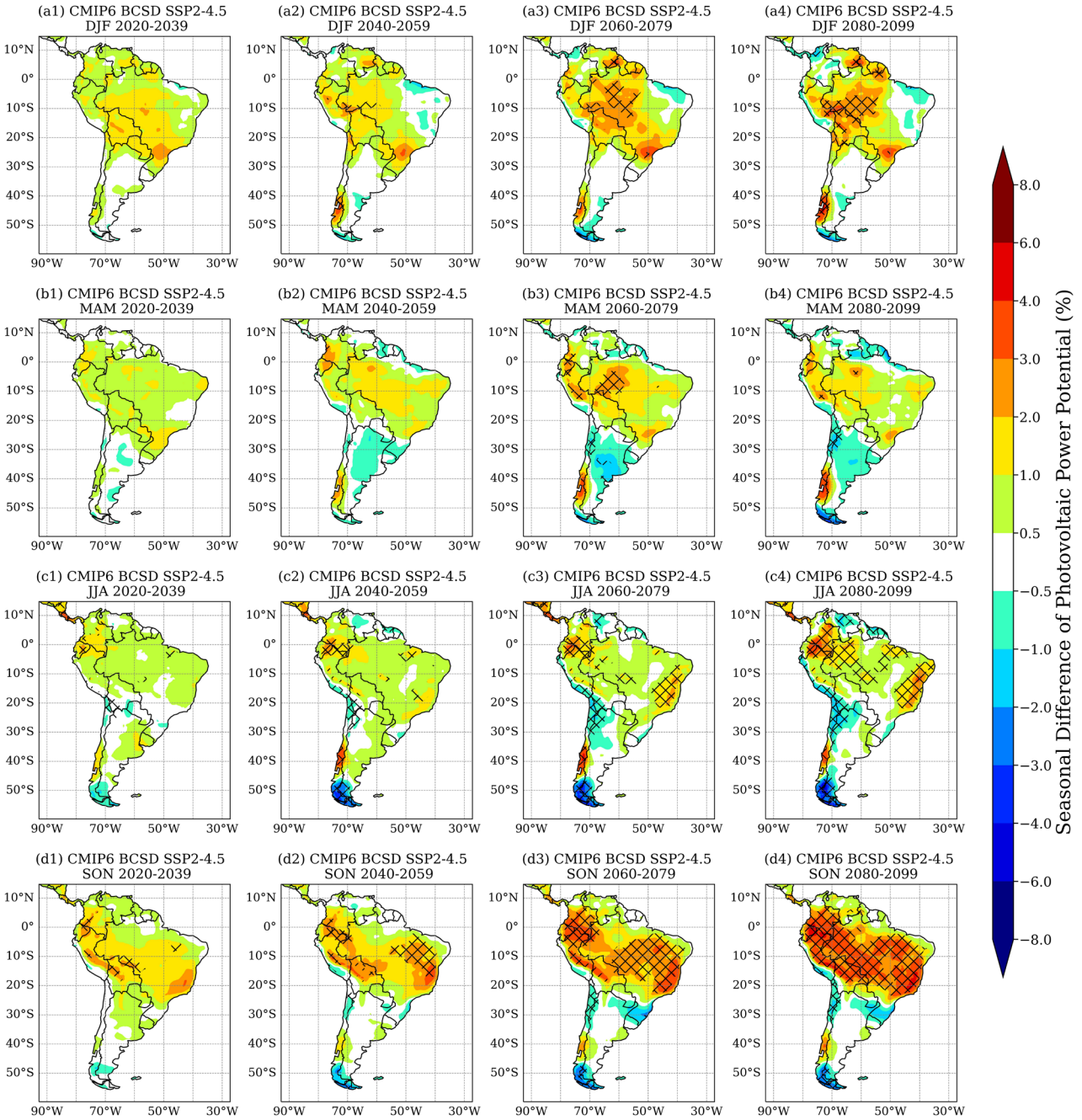


Figure 8. Seasonal difference (%) in PVP_{pot} projected by the CMIP6 ensemble after BCSD with the CLARA-A3 + ERA5 ensemble under the SSP2-4.5 emission scenario for the periods 2020–2039, 2040–2059, 2060–2079, and 2080–2099 in relation to the historical period (1995-2014). Hatched areas indicate a statistical significance of 95%, based on the Student's *t*-test.

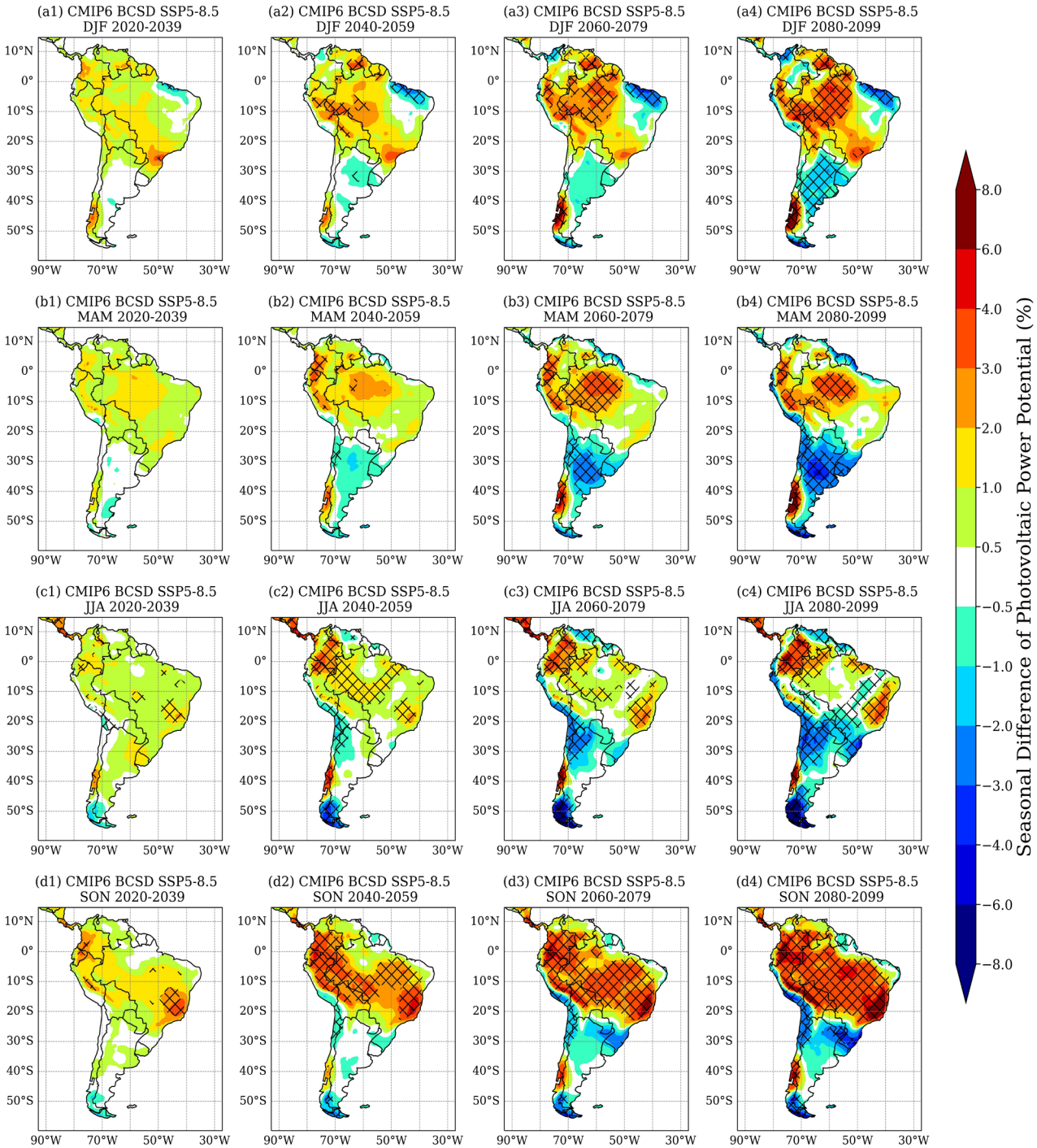


Figure 9. Similar to **Figure 8**, except for the SSP5-8.5 scenario.

For the SON months, under both scenarios, the CMIP6 ensemble shows significant increases of 2 to 6% by 2059 in the Brazilian Midwest, the northern portion of Northeast Brazil, the coast of Southeast Brazil, Brazilian Amazonia, Bolivia, Peru, Ecuador, and Colombia, reiterating previous CMIP6 results for 2015–2040 under the same scenarios [22]. From 2060 onwards, both scenarios amplify the regions with a significant increase above 3%, covering practically all of Brazil, Bolivia, Peru, Colombia, Ecuador, and Venezuela, with the SSP5-8.5 scenario showing a more intense sign of change. These results corroborate CMIP6 projections already made for 2041–2100, which indicate a transversal range of increasing PVP of up to 8% extending from the coast of southeastern Brazil to the north of SA [22].

In summary, results indicated that regions with solar energy potential in the historical period maintain suitable conditions in the future climate. Furthermore, the projections of CSP suggest an increasing generation in most SA (mainly Brazil, Peru, Bolivia, Ecuador, and Colombia). On the other hand, although PVP projections also majoritarily indicate favorable conditions for solar energy generation (especially during SON and under the SSP5-8.5 scenario), there are decreasing estimates in areas such as the northern sector of the Brazilian Northeast (during DJF), southern Brazil, Argentina and north Chile (all year round), whose reduction sign is more intense under the SSP5-8.5 scenario, which was also observed in studies with projections of CMIP3 [14], CMIP5 [18,19,30,31] and CMIP6 [22,24,32] models. In general, the negative PVP anomalies obtained here partially agree with those of other studies, which found that a thermal increase of up to 5 °C under the RCP-8.5 scenario can promote a reduction of up to 3% in PVP generation [15,17]. Thus, we suggest that the decreasing PVP in these regions may stem from the increasing local warming, given that the efficiency of PVP solar panels reduces by approximately 0.2–0.5% for every 1 °C increase in temperature [10,69]. However, in other regions where local warming does not result in negative PVP projections, it is likely that other factors, such as increased solar irradiance at the surface and reduced cloud cover, can compensate for this decrease in the PVP panels' efficiency due to thermal warming [15,24]. In this sense, the decreasing cloud cover projected for low latitudes [70] and the increasing average surface wind speed of 0.5–1.0 m s^{-1} estimated for SA [40] may enhance the PVP generation, contributing to greater solar panel efficiency (through the higher incidence of solar radiation and the cooling effect). Moreover, the projections of increasing cloud cover in mid-latitudes [70] and precipitation in southern Brazil [39] may intensify the decreasing PVP in South Brazil for the coming decades.

We stress that errors persist in climate simulations even after bias correction of the original CMIP6 data. One reason for this arises from the CM SAF CLARA-A3 solar irradiance at the surface being derived from other parameters such as the cloud cover index (extracted from satellite observations), vertically integrated water vapor, ozone, and surface albedo (obtained from climatological data from ERA5) through a radiative transfer model, which also has their associated biases and uncertainties [21,54]. However, we highlight the good performance of the QDM technique in reducing the systematic errors of CMIP6 simulations by up to 50% when using the CLARA-A3 + ERA5 ensemble mean for statistical downscaling.

Anomalies time series and trends

Figures 10 to **13** present the seasonal PVP_{pot} anomalies (in percentage) in six subdomains of SA projected by each CMIP6 GCM and the multi-model ensemble under the SSP5-8.5 scenario and after BCSD with the CLARA-A3 + ERA5 ensemble mean. The series represents seasonal anomalies projected for 2020-2099 relative to the climatological period (1995–2014). In addition, **Tables 2** to **5** also present the results of the Mann-Kendall and Sen's slope tests, provided by each model and the multi-model ensemble for the six subdomains under the SSP5-8.5 scenario.

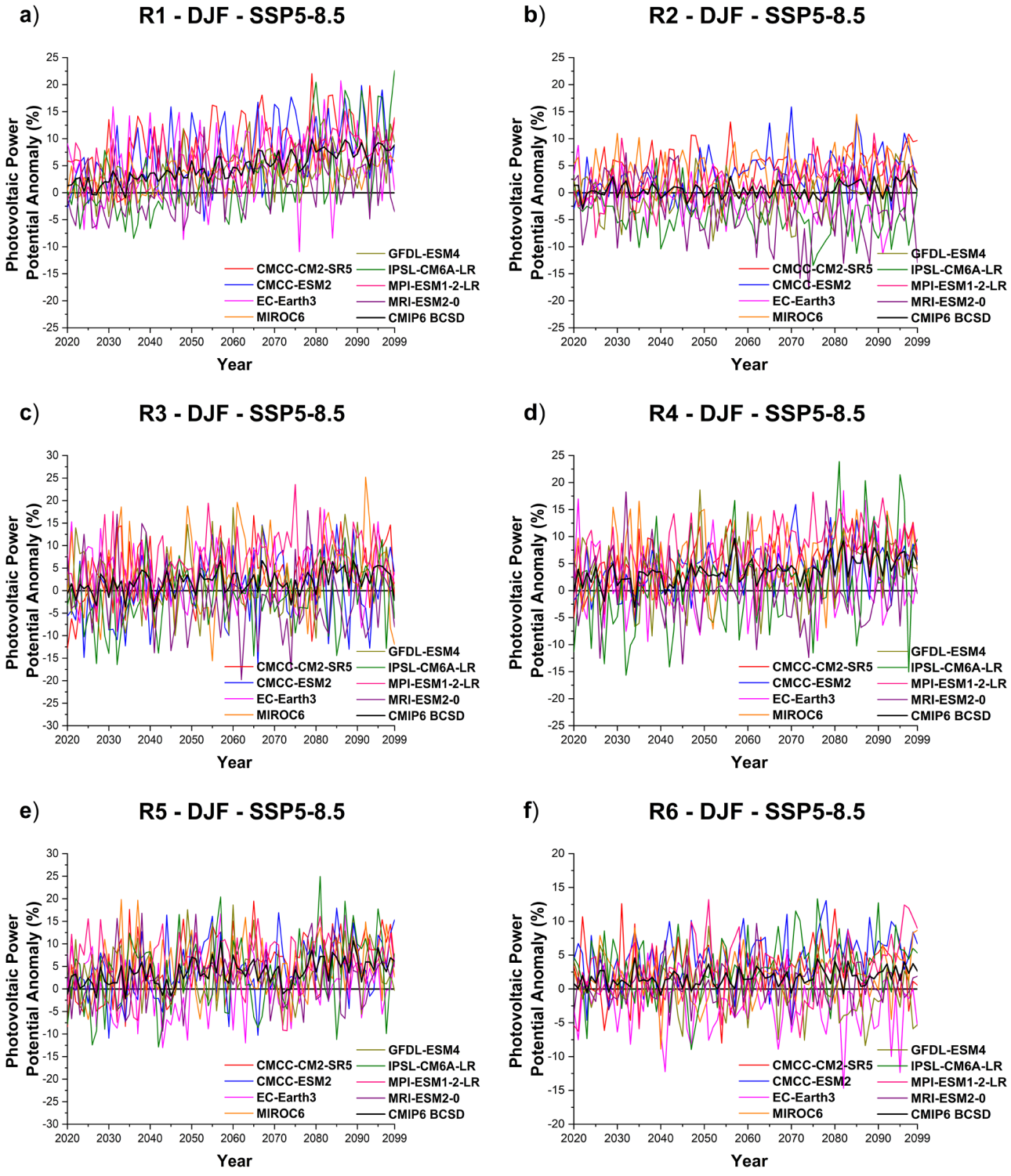


Figure 10. Time series (2020–2099) of PVP_{pot} anomalies (%) in the DJF months for six SA subdomains (R1-R6) relative to the climatological period (1995–2014), obtained after BCSD with the CLARA-A3 + ERA5 ensemble under the SSP5-8.5 scenario.

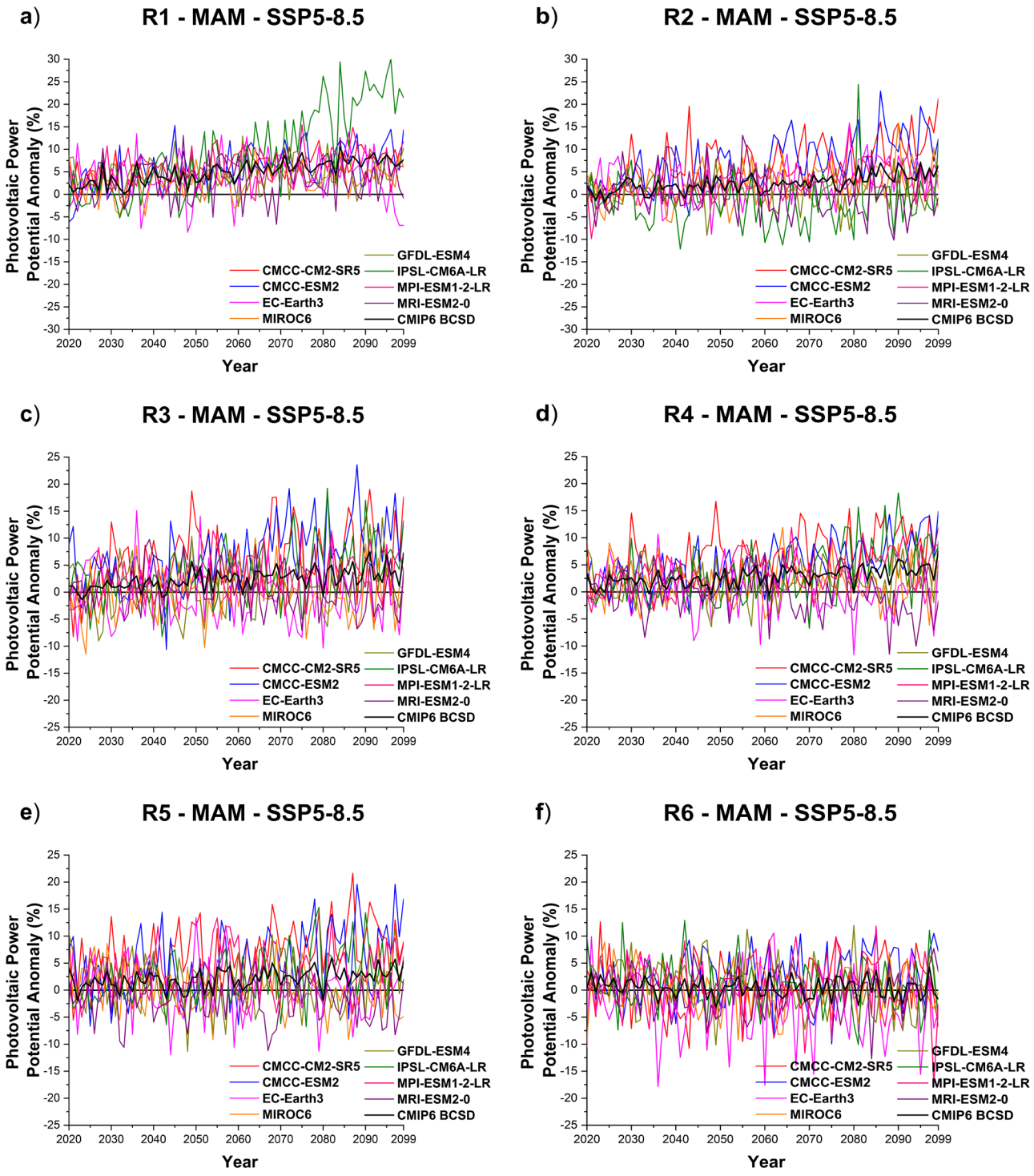


Figure 11. Similar to **Figure 10**, except for MAM.

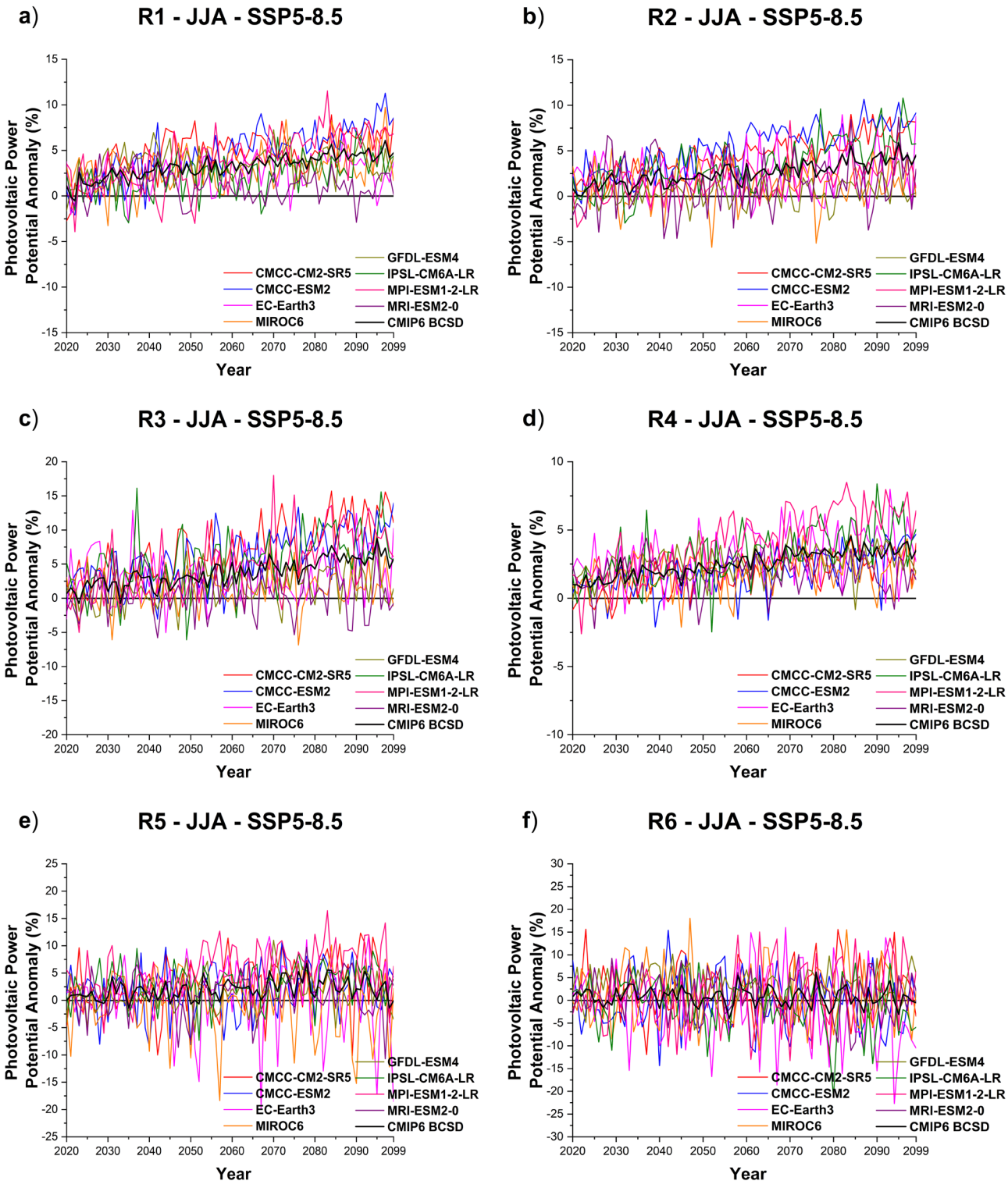


Figure 12. Similar to **Figure 10**, except for JJA.

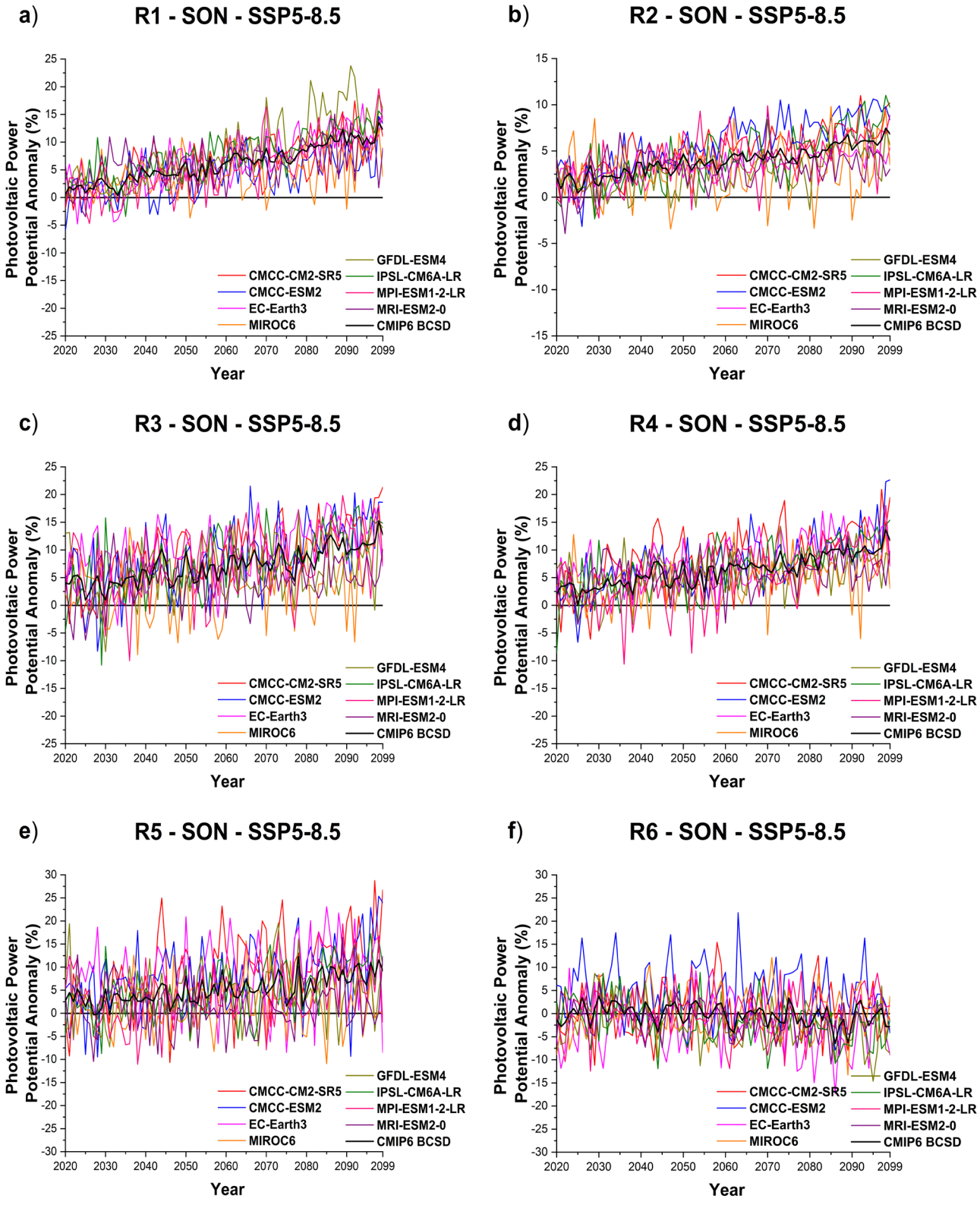


Figure 13. Similar to **Figure 10**, except for SON.

Table 2. Parameters of the Mann-Kendall and Sen's Slope tests for the PVP_{pot} time series in the months of DJF (2020–2099) for six SA subdomains obtained by each GCM and CMIP6 multi-model ensemble after BCSD and under the SSP5-8.5 scenario. P, N, NT, T, and F denote positive, negative, no trend, true and false, respectively.

		CMCC-SR5	CMCC-ESM2	EC-EARTH3	MIROC6	GFDL-ESM4	IPSL-CM6A-LR	MPI-ESM1-2-LR	MRI-ESM2-0	CMIP6 BCSD
R1	Trend	P	P	NT	P	NT	P	P	P	P
	Ho	T	T	F	T	F	T	T	T	T
	Slope	0.0295	0.0241	0.0127	0.0100	0.0173	0.0324	0.0245	0.0162	0.0192
R2	Trend	P	P	NT	P	NT	N	P	N	NT
	Ho	T	T	F	T	F	T	T	T	F
	Slope	0.0133	0.0178	–0.0059	0.0098	0.0068	–0.0087	0.0151	–0.0181	0.0035
R3	Trend	P	P	NT	NT	NT	P	P	N	P
	Ho	T	T	F	F	F	T	T	T	T
	Slope	0.0228	0.0200	0.0022	0.0153	0.0138	0.0173	0.0200	0.0196	0.0105
R4	Trend	P	P	NT	NT	NT	P	P	NT	P
	H_o	T	T	F	F	F	T	T	F	T
	Slope	0.0182	0.0164	–0.0024	0.0106	0.0064	0.0283	0.0247	–0.0050	0.0119
R5	Trend	P	P	NT	NT	NT	P	NT	NT	P
	H_o	T	T	F	F	F	T	F	F	T
	Slope	0.0342	0.0221	0.0054	0.0113	0.0081	0.0223	0.0101	0.0074	0.0145
R6	Trend	P	P	NT	NT	N	P	P	NT	P
	H_o	T	T	F	F	T	T	T	F	T
	Slope	0.0115	0.0123	0.0058	0.0041	–0.0119	0.0139	0.0169	0.0030	0.0053

Table 3. Similar to **Table 2**, except for the MAM months.

		CMCC-SR5	CMCC-ESM2	EC-EARTH3	MIROC6	GFDL-ESM4	IPSL-CM6A-LR	MPI-ESM1-2-LR	MRI-ESM2-0	CMIP6 BCSD
R1	Trend	P	P	NT	P	NT	P	P	NT	P
	Ho	T	T	F	T	F	T	T	F	T
	Slope	0.0133	0.0211	0.0035	0.0085	0.0030	0.0619	0.0169	0.0025	0.0100
R2	Trend	P	P	NT	P	NT	NT	P	NT	P
	Ho	T	T	F	T	F	F	T	F	T
	Slope	0.0277	0.0306	0.0079	0.0140	–0.0004	–0.0005	0.0166	–0.0076	0.0114
R3	Trend	P	P	NT	NT	NT	P	NT	NT	P
	Ho	T	T	F	F	F	T	F	F	T
	Slope	0.0226	0.0254	–0.0032	0.0001	0.0078	0.0171	0.0143	–0.0098	0.0098
R4	Trend	P	P	NT	NT	NT	P	P	N	P
	H_o	T	T	F	F	F	T	T	T	T
	Slope	0.0188	0.0244	–0.0053	–0.0015	0.0047	0.0235	0.0172	–0.0103	0.0089
R5	Trend	P	P	NT	N	NT	P	NT	NT	P
	H_o	T	T	F	T	F	T	F	F	T
	Slope	0.0194	0.0236	–0.0031	–0.0085	–0.0001	0.0153	0.0081	–0.0049	0.0062
R6	Trend	NT	NT	NT	NT	N	NT	NT	NT	NT
	H_o	F	F	F	F	T	F	F	F	F
	Slope	0.0057	0.0065	–0.0044	–0.0033	–0.0092	–0.0026	–0.0028	0.0006	–0.0023

Table 4. Similar to **Table 2**, except for the JJA months.

		CMCC-SR5	CMCC-ESM2	EC-EARTH3	MIROC6	GFDL-ESM4	IPSL-CM6A-LR	MPI-ESM1-2-LR	MRI-ESM2-0	CMIP6 BCSD
R1	Trend	P	P	P	P	P	P	P	NT	P
	Ho	T	T	T	T	T	T	T	F	T
	Slope	0.0139	0.0220	0.0065	0.0063	0.0044	0.0099	0.0187	-0.0019	0.0100
R2	Trend	P	P	NT	NT	P	P	P	NT	P
	Ho	T	T	F	F	T	T	T	F	T
	Slope	0.0195	0.0220	0.0009	0.0029	0.0034	0.0187	0.0116	0.0038	0.0108
R3	Trend	P	P	NT	NT	P	P	P	NT	P
	Ho	T	T	F	F	T	T	T	F	T
	Slope	0.0281	0.0234	0.0044	0.0043	0.0072	0.0166	0.0267	0.0014	0.0136
R4	Trend	P	P	P	NT	P	P	P	NT	P
	H_o	T	T	T	F	T	T	T	F	T
	Slope	0.0101	0.0092	0.0067	0.0031	0.0046	0.0118	0.0167	0.0002	0.0078
R5	Trend	P	NT	NT	NT	NT	P	P	NT	P
	H_o	T	F	F	F	F	T	T	F	T
	Slope	0.0172	0.0063	-0.0005	-0.0024	0.0050	0.0075	0.0167	0.0147	0.0045
R6	Trend	NT	NT	NT	NT	NT	N	P	NT	NT
	H_o	F	F	F	F	F	T	T	F	F
	Slope	0.0021	–0.0028	–0.0098	0.0006	–0.0018	–0.0067	0.0106	–0.0015	–0.0013

Table 5. Similar to **Table 2**, except for the SON months.

		CMCC-SR5	CMCC-ESM2	EC-EARTH3	MIROC6	GFDL-ESM4	IPSL-CM6A-LR	MPI-ESM1-2-LR	MRI-ESM2-0	CMIP6 BCSD
R1	Trend	P	P	P	P	P	P	P	P	P
	Ho	T	T	T	T	T	T	T	T	T
	Slope	0.0295	0.0227	0.0389	0.0133	0.0449	0.0379	0.0379	0.0171	0.0304
R2	Trend	P	P	P	NT	P	P	P	NT	P
	Ho	T	T	T	F	T	T	T	F	T
	Slope	0.0211	0.0291	0.0119	0.0038	0.0162	0.0290	0.0184	0.0047	0.0169
R3	Trend	P	P	P	P	P	P	P	NT	P
	Ho	T	T	T	T	T	T	T	F	T
	Slope	0.0413	0.0404	0.0261	0.0169	0.0137	0.0416	0.0288	0.0097	0.0279
R4	Trend	P	P	P	P	P	P	P	NT	P
	H_o	T	T	T	T	T	T	T	F	T
	Slope	0.0368	0.0337	0.0292	0.00139	0.0186	0.0378	0.0282	0.0079	0.0261
R5	Trend	P	P	NT	NT	NT	P	P	NT	P
	H_o	T	T	F	F	F	T	T	F	T
	Slope	0.0465	0.0318	0.0141	0.0105	0.0095	0.0324	0.0184	0.0017	0.0203
R6	Trend	NT	NT	NT	NT	N	N	NT	N	N
	H_o	F	F	F	F	T	T	F	T	T
	Slope	0.0007	–0.0081	–0.0056	0.0058	–0.0179	–0.0161	0.0072	–0.0101	–0.0063

For R1, approximately 83% of PVP anomaly projections are positive, indicating year-round solar potential growth in the region throughout the 21st century. Considering all seasons, only the EC-Earth3, GFDL-ESM4, and MRI-ESM2-0 models do not project a significant positive trend in PVP in the Amazonia sector. Similarly, the multi-model ensemble projects a significant increase in year-round PVP throughout the 21st century, with anomalies of up to 13.5% in SON months. EC-Earth3, IPSL-CM6A-LR, and MPI-ESM1-2-LR models present the largest amplitude of projected PVP anomalies in the months of DJF, MAM, JJA, and SON, respectively. On the other hand, the maximum PVP anomalies are projected by the models IPSL-CM6A-LR (~23% in DJF 2099 and ~30% in MAM 2096), MPI-ESM1-2-LR (~11.5% in JJA from 2083) and GFDL-ESM4 (~28% in SON from 2091). Other studies also indicate a significant increase in PVP in the region throughout the century, projected by CMIP3 [14], CMIP5 [18,19,24,30,31], and CMIP6 [22,24] models.

For R2, approximately 61% of projections indicate a statistically significant increase in year-round PVP during the 21st century. EC-Earth3, GFDL-ESM4, IPSL-CM6A-LR, and MRI-ESM2-0 models indicate no trend or negative trend in the months of DJF and MAM, while in the months of JJA and SON, EC-Earth3, MIROC6, and MRI-ESM2-0 models do not indicate a significant trend. Similarly, the CMIP6 multi-model ensemble projects a statistically significant increase in PVP in all months, with a positive anomaly of up to 7.5% in MAM 2098. MRI-ESM2-0, CMCC-ESM2, and IPSL-CM6A-LR models present the largest range of projections, while the largest seasonal PVP anomalies show increases of up to 16% in 2070 DJF (CMCC-ESM2), 23% in 2081 MAM (CMCC-ESM2), 11% in 2096 JJA (IPSL-CM6A-LR) and 11% in 2092 SON (IPSL-CM6A-LR).

Regarding R3, around 64% of projections indicate a statistically significant increase in PVP throughout the year during the 21st century. EC-Earth3, GFDL-ESM4, MIROC6, IPSL-CM6A-LR, MPI-ESM1-2-LR, and MRI-ESM2-0 show no trend in practically the entire year, while for the SON months, only the MRI-ESM2-0 model does not indicate a significant positive trend. Furthermore, the ensemble projects an increase of up to 17% in the SON months of 2098. The CMCC-ESM2, MIROC6, and MPI-ESM1-2-LR models have the largest range of projections, with the MPI-ESM1-2-LR model projecting a positive PVP anomaly of ~25% in DJF of 2092. In general, the anomalies projected by the models and ensemble agree with those of other studies that show an average increase of 5% in the PVP of the northeastern region for the following decades, projected by models of CMIP5 [19,30,24] and CMIP6 [22].

For R4, approximately 70% of projections estimate a significant increase in PVP throughout the year during the following decades, while EC-Earth3, MIROC6, GFDL-ESM4, and MRI-ESM2-0 models indicate no trend or negative trend in practically all year. Furthermore, the ensemble projects a statistically significant increase in PVP throughout the year, with a positive anomaly of up to 14% during SON of 2098. CMCC-ESM2, IPSL-CM6A-LR, and MPI-ESM1-2-LR models present greater amplitude of projections, estimating up to 24% increases in the DJF months. The anomalies obtained corroborate the average growth of approximately 5% in the PVP of the Brazilian Midwest during the 21st century, estimated by CMIP5 models under the RCP4.5 [19] and RCP8.5 [30] scenarios and CMIP6 under the SSP2-4.5 and SSP5-8.5 scenarios [22].

Regarding R5, approximately 47% of projections indicate a statistically significant increase in PVP throughout the year during the 21st century. Similar to regions R3 and R4, in this sector, EC-Earth3, GFDL-ESM4, MIROC6, IPSL-CM6A-LR, MPI-ESM1-2-LR, and MRI-ESM2-0 result in no trend in seasonal PVP projections across most of the year. Furthermore, the CMIP6 ensemble projects a statistically significant increase in PVP throughout the year, with a positive anomaly of up to 12% in the SON months. IPSL-CM6A-LR, CMCC-CM2-SR5, and EC-Earth3 models present the largest range of projections, with the CMCC-CM2-SR5 and IPSL-CM6A-LR GCMs estimating increases of up to 28% and 25% in the

months of SON and DJF, respectively. Similarly, the anomalies found here reiterate those of other studies, which obtained an average increase of 5% in PVP for the coming decades in Southeast Brazil, projected by CMIP5 [19,30,31] and CMIP6 [22,24] models.

Finally, for R6, only 16% of projections estimate a significant increase in PVP, concentrated in the DJF months. Unlike the other five regions evaluated, the projections obtained for South Brazil and Uruguay mainly indicate a non-significant or negative trend in PVP throughout the year for the coming decades. Furthermore, the CMIP6 ensemble projects a statistically significant increase (reduction) in PVP only in DJF (SON). In general, these results corroborate the literature since the considerable decrease of PVP in South Brazil was also estimated by projections from CMIP3 [14], CMIP5 [18,19,24,30], and CMIP6 [22,24,32].

In summary, PVP trend analyses in different subdomains of SA show that practically all regions (except the southern region of Brazil and Uruguay) show a tendency for an increasing solar potential during the 21st century throughout the year (with better estimates for the austral spring and summer and sectors R1 and R4). The anomaly projections obtained by the ensemble show that, in descending order, the most significant increases in PVP occur in northern Brazil (R1), Brazilian Midwest (R4), southern and central sectors of Northeast Brazil (R3), north sector of Northeast Brazil (R2) and Southeast Brazil (R5). On the other hand, southern Brazil (R6) presents around 84% of projections with a negative trend or no signal, highlighting an unfavorable or uncertain scenario for the PVP development in the region.

In general, the models mostly converge to an increasing PVP throughout the century in practically all of Brazil. On the other hand, while models such as EC-Earth3 and MIROC6 result in no trend in almost all analyses, other GCMs such as GFDL-ESM4 and MRI-ESM2-0 project mixed signals, depending on the regions and seasons. In any case, the projections reiterate the literature, which shows a significant increasing tendency for PVP over the next decades in the Amazonia region [14,18,19,22,24,30,31,32], the Northeast, Midwest, and Southeast Brazil [19,22,24,30,31]. Conversely, projections for South Brazil predominantly suggest the absence of a signal or a tendency towards a decreasing PVP, corroborating previous results [14,19,22,24,30,31,32].

4. Conclusions

The growing demand for energy makes it urgent to promote sustainable development in response to climate change. In this context, adopting measures to mitigate environmental impacts is essential to promote the efficient use of resources and the clean energy transition. Therefore, this study sought to evaluate the projections of change in solar irradiance, concentrated solar energy, and photovoltaic energy potential estimated by an ensemble of eight CMIP6 GCMs for SA during the 21st century under the SSP2-4.5 and SSP5-8.5 scenarios. To this end, we applied statistical downscaling to the simulations and projections of the CMIP6 models using the ERA5 reanalysis and CLARA-A3 satellite observations as reference data. The ERA5 + CLARA-A3 ensemble mean validated the climate simulations for the historical period (1995–2014) and the application of statistical downscaling. The QDM technique effectively reduced the systematic biases of the original CMIP6 solar irradiance simulations, reducing errors by approximately 50% over practically the entire continent throughout the year. However, even after the BCSD method, biases persist in regions such as northeastern Brazil and northern SA.

The projections of CSP show that regions traditionally favorable to its generation (mainly the Brazilian Northeast) may maintain suitable conditions in the coming decades. On the other hand, projections of decreasing PVP in sectors such as the north of the Brazilian Northeast, Argentina, the west coast of SA, and southern Brazil suggest that other climate factors such as local warming, cloud cover, aerosols, and wind speed may influence solar energy generation in these regions. In general, the results indicate spatial and seasonal variability of solar generation in SA, pointing to increases of approximately 1–6% in CSP (mainly under the SSP5-8.5 scenario in southern Chile and most of Brazil) and 1–4% in PVP gen-

eration (mainly under the SSP5-8.5 scenario in the Amazon, Midwest and Southeast Brazilian sectors). In addition, trend analyses projected individually by the CMIP6 GCMs converge on an increasing PVP, mainly in Brazil's Amazonia and Midwest regions. Conversely, for the country's southern sector, approximately 84% of the projections show a negative trend (or no trend), showing unfavorable or uncertain conditions for the development of PVP generation in the region.

It is also worth mentioning some limitations of this study. Firstly, this analysis investigates the possible changes in solar energy generation in SA from a purely atmospheric perspective without considering other relevant economic, technological, and political factors. In this sense, future research should consider the feasibility of expanding the solar matrix on the continent through incentive policies for the sector that favor strategic planning, foreign investment, solar industry consolidation, and energy storage. Furthermore, there is no analysis of the technological advances that may improve the photovoltaic panels' efficiency (including their performance concerning thermal heating) and the reduced cost of solar technology, factors that could encourage its implementation in SA over the coming decades. In addition, we highlight the importance of studies that evaluate the relationship between solar energy generation and cloud cover, given that in SA, this correspondence is well corroborated during the austral fall and inconsistent for the other seasons [22]. In this context, regional climate models are valuable tools for analyzing this issue, and we expect to see increasing use of these models driven by CMIP6 GCMs in future research.

Finally, we point out that the datasets used to validate climate simulations also have their systematic biases. Although the reanalysis products have satisfactory overall performance, these data result from the assimilation of observations and numerical simulations through radiative transfer models [52], so uncertainties and biases are inherent to this source of information. For example, the solar energy derived from the ERA5 reanalysis is overestimated by approximately 23% during the boreal winter in North America [54]. Furthermore, one of SA's solar hotspots (Northeast Brazil) corresponds to one of the global sectors where CLARA-A3 presents uncertainties [55]. Here, we stress that the satellite dataset also has systematic biases since it derives from the assimilation of different sources, such as reanalysis and numerical simulations [21,55]. Given this, we reiterate that the projections must be analyzed considering the uncertainties and systematic biases of the reference data.

Moreover, this study uses CMIP6 climate projections with bias correction and statistical downscaling to assess solar potential in SA. Generally, studies analyze raw model outputs with coarse resolution and without bias correction, which is inappropriate for studies focused on renewable energy and climate change impacts. In this context, our results advance knowledge about future solar generation scenarios on the continent and represent a first look at solar energy potential in SA with corrected state-of-the-art projections. Furthermore, the few existing studies on the future potential of solar energy with CMIP6 models in South America evaluate shorter time horizons, such as the near future of 2021–2050 [32] and the distant future of 2071–2100 [24]. In this sense, our study differs by presenting projections for the entire 21st century, using four time horizons of interest to the South American energy sector.

Nevertheless, the projections presented here may have significant implications for policymakers, energy planners, and South American energy sector investors. For instance, indicating areas with high solar power potential underscores promising locales for establishing solar farms, fostering strategic planning, and assisting the transition towards a low-carbon and sustainable energy grid across SA. Lastly, this study gives helpful insights to stakeholders engaged in developing the solar energy infrastructure, as the analyses herein mark a fresh analysis of statistically downscaled climate projections from CMIP6 models tailored to SA's solar potential.

Author Contributions

Glauber W.S. Ferreira, Michelle S. Reboita, and

J.G.M. Ribeiro processed and analyzed the data. Glauber W.S. Ferreira and Michelle S. Reboita wrote the original draft. All authors read and approved the final manuscript.

Conflict of Interest

The authors have no relevant financial or non-financial interests to disclose.

Funding

This research was funded by Engie Brasil Energia (R&D00403–54/2022) through the R&D Program regulated by the Brazilian Electricity Regulatory Agency (ANEEL) and the Coordination for the Improvement of Higher Education (CAPES, Finance Code 001).

Acknowledgments

The authors thank the National Council for Scientific and Technological Development (CNPq), Coordination for the Improvement of Higher Education (CAPES), and Engie Brasil Energia for their financial support. The authors also thank the European Centre for Medium-Range Weather Forecasts (ECMWF), the Coupled Model Intercomparison Project (CMIP), and the Satellite Application Facility on Climate Monitoring (CM SAF) from the European Organization for the Exploitation of Meteorological Satellites (EUMETSAT) for the data used in this study.

Data Availability Statement

The CMIP6 climate models are available at: https://aims2.llnl.gov/search/cmip6/. The ECMWF-ERA5 reanalysis is available at: https://cds.climate.copernicus.eu/. Satellite observations from CLARA–A3 are available at: https://wui.cmsaf.eu/safira/action/viewProduktList?dId=2

References

[1] Climate Change 2023: Synthesis Report. IPCC: Geneva, Switzerland. pp. 1–34. DOI: https://doi.org/10.59327/IPCC/AR6-9789291691647.001

[2] Reboita, M.S., Ambrizzi, T., 2022. Climate system in a nutshell: an overview for understanding climate change. International Journal of Development Research. 12, 53365-53378. Available from: https://www.journalijdr.com/sites/default/files/issue-pdf/23731.pdf

[3] Climate Change: Global Temperature [Internet] [cited 2024 Apr 3]. Available from: https://www.energy.gov/sites/default/files/2024-02/093.%20Rebecca%20Lindsey%20and%20Luann%20Dahlman%2C%20NOAA%2C%20Climate%20Change_%20Global%20Temperature.pdf

[4] Icaza, D., Borge-Diez, D., Galindo, S.P., 2022. Analysis and proposal of energy planning and renewable energy plans in South America: Case study of Ecuador. Renewable Energy. 182, 314–342. DOI: https://doi.org/10.1016/j.renene.2021.09.126

[5] Arango-Aramburo, S., Ríos-Ocampo, J.P., Larsen, E.R., 2020. Examining the decreasing share of renewable energy and growing thermal capacity: The case of South America. Renewable and Sustainable Energy Review. 119, 109648. DOI: https://doi.org/10.1016/j.rser.2019.109648

[6] Deng, Q., Alvarado, R., Toledo, E., Caraguay, L., 2020. Greenhouse gas emissions, non-renewable energy consumption, and output in South America: the role of the productive structure. Environmental Science and Pollution Research. 27, 14477–14491. DOI: https://doi.org/10.1007/s11356-020-07693-9

[7] A Race to the Top Latin America 2023: Wind and Solar Utility-Scale Buildout Gains Speed in Brazil, Chile and Colombia, while Mexico Falls Behind [Internet] [cited 2024 Apr 5]. Available from: https://globalenergymonitor.org/report/a-race-to-the-top-latin-america/

[8] Brazil Holds the Key to Latin America's Solar Potential [Internet] [cited 2024 Apr 5].

Available from: https://www.reuters.com/markets/commodities/brazil-holds-key-latin-americas-solar-potential-2024-02-29/#:~:text=PV%20PLANS,of%20Latin%20America's%20solar%20generation

[9] Exame, E.S.G., 2024. Solar Energy Reaches 40 GW of Installed Capacity in Brazil. Retrieved from Exame ESG [Internet] [cited 2024 Apr 5]. Available from: https://exame.com/esg/energia-solar-alcanca-40-gw-de-capacidade-instalada-no-brasil/ (In Portuguese)

[10] Patt, A., Pfenninger, S., Lilliestam, J., 2013. Vulnerability of solar energy infrastructure and output to climate change. Climatic Change. 121, 93–102.
DOI: https://doi.org/10.1007/s10584-013-0887-0

[11] Solar Energy [Internet] [cited 2024 Apr 5]. Available from: https://www.irena.org/Energy-Transition/Technology/Solar-energy

[12] Letcher, T.M., 2022. Comprehensive renewable energy, 2nd ed. Elsevier: Amsterdam, Netherlands. pp. 796.

[13] Solar Energy Becomes the Third Largest Source in Brazil [Internet] [cited 2024 Apr 5]. Available from: https://www.gov.br/en/government-of-brazil/latest-news/solar-energy-becomes-the-third-largest-source-in-brazil

[14] Crook, J.A., Jones, L.A., Forster, P.M., et al., 2011. Climate change impacts on future photovoltaic and concentrated solar power energy output. Energy & Environmental Science. 4, 3101.
DOI: https://doi.org/10.1039/c1ee01495a

[15] Jerez, S., Tobin, I., Vautard, R., et al, 2015. The impact of climate change on photovoltaic power generation in Europe. Nature Communications. 6, 10014.
DOI: https://doi.org/10.1038/ncomms10014

[16] Wild, M., Folini, D., Henschel, F., Fischer, N., Müller, B., 2015. Projections of long-term changes in solar radiation based on CMIP5 climate models and their influence on energy yields of photovoltaic systems. Solar Energy. 116, 12–24.
DOI: https://doi.org/10.1016/j.solener.2015.03.039

[17] Müller, J., Folini, D., Wild, M., et al., 2019. CMIP-5 models project photovoltaics are a no-regrets investment in Europe irrespective of climate change. Energy. 171, 135–148.
DOI: https://doi.org/10.1016/j.energy.2018.12.139

[18] Zou, L., Wang, L., Li, J., et al., 2019. Global surface solar radiation and photovoltaic power from Coupled Model Intercomparison Project Phase 5 climate models. Journal of Cleaner Production. 224, 304–324.
DOI: https://doi.org/10.1016/j.jclepro.2019.03.268

[19] Feron, S., Cordero, R.R., Damiani, A., et al., 2021. Climate change extremes and photovoltaic power output. Nature Sustainability. 4, 270–276.
DOI: https://doi.org/10.1038/s41893-020-00643-w

[20] Gernaat, D.E.H.J., de Boer, H.S., Daioglou, V., Yalew, S.G., Müller, C., van Vuuren, D.P., 2021. Climate change impacts on renewable energy supply. Nature Climate Change. 11, 119-125.
DOI: https://doi.org/10.1038/s41558-020-00949-9

[21] Sawadogo, W., Reboita, M.S., Faye, A., et al, 2021. Current and future potential of solar and wind energy over Africa using the RegCM4 CORDEX-CORE ensemble. Climate Dynamics. 57, 1647–1672.
DOI: https://doi.org/10.1007/s00382-020-05377-1

[22] Dutta, R., Chanda, K., Maity, R., 2022. Future of solar energy potential in a changing climate across the world: A CMIP6 multimodel ensemble analysis. Renewable Energy. 188, 819–829.
DOI: https://doi.org/10.1016/j.renene.2022.02.023

[23] Ndiaye, A., Moussa, M.S., Dione, C., et al., 2023. Projected changes in solar PV and wind energy potential over West Africa: an analysis of CORDEX-CORE simulations. Energies. 15,

9602.
DOI: https://doi.org/10.3390/en15249602

[24] Ha, S., Zhou, Z., Im, E.-S., et al., 2023. Comparative assessment of future solar power potential based on CMIP5 and CMIP6 multimodel ensembles. Renewable Energy. 206, 324–335.
DOI: https://doi.org/10.1016/j.renene.2023.02.039

[25] Barbosa, L.S.N.S., Bogdanov, D., Vainikka, P., et al., 2017. Hydro, wind and solar power as a base for a 100% renewable energy supply for South and Central America. PLoS ONE. 12, e0173820.
DOI: https://doi.org/10.1371/journal.pone.0173820

[26] Gil, G.M.V., Cunha, R.B.A., Di Santo, S.G., et al, 2020. Photovoltaic energy in South America: Current state and grid regulation for large-scale and distributed photovoltaic systems. Renewable Energy. 162, 1307–1320.
DOI: https://doi.org/10.1016/j.renene.2020.08.022

[27] Narvaez, G., Giraldo, L.F., Bressan, M., 2022. The impact of climate change on photovoltaic power potential in Southwestern Colombia. Heliyon. 8, e11122.
DOI: https://doi.org/10.1016/j.heliyon.2022.e11122

[28] Lopez, G., Aghahosseini, A., Bogdanov, D., et al, 2021. Pathway to a fully sustainable energy system for Bolivia across power, heat, and transport sectors by 2050. Journal of Cleaner Production. 293, 126195.
DOI: https://doi.org/10.1016/j.jclepro.2021.126195

[29] Osorio-Aravena, J.C., Aghahosseini, A., Bogdanov, D., et al, 2021. The impact of renewable energy and sector coupling on the pathway towards a sustainable energy system in Chile. Renewable and Sustainable Energy Reviews. 151, 111557.
DOI: https://doi.org/10.1016/j.rser.2021.111557

[30] de Jong, P., Barreto, T.B., Tanajura, C.A.S., et al, 2019. Estimating the impact of climate change on wind and solar energy in Brazil using a South American regional climate model. Renewable Energy. 141, 390–401.
DOI: https://doi.org/10.1016/j.renene.2019.03.086

[31] Costa, R.S., da Costa, G.L., de Lima, F.J.L., et al, 2020. Impacts of climate change on the availability of solar energy resources. Revista Brasileira de Energia. 26, 39–50. (In Portuguese)
DOI: https://doi.org/10.47168/rbe.v26i4.579

[32] Zuluaga, C.F., Avila-Diaz, A., Justino, F.B., et al, 2022. The climate change perspective of photovoltaic power potential in Brazil. Renewable Energy. 193, 1019–1031.
DOI: https://doi.org/10.1016/j.renene.2022.05.029

[33] Ambrizzi, T., Reboita, M.S., da Rocha, R.P., et al., 2019. The state of the art and fundamental aspects of regional climate modeling in South America. Annals of the New York Academy of Sciences. 1436, 98–120.
DOI: https://doi.org/10.1111/nyas.13932

[34] Mutz, S.G., Scherrer, S., Muceniece, I., et al., 2021. Twenty-frst century regional temperature response in Chile based on empirical-statistical downscaling. Climate Dynamics. 56, 2881–2894.
DOI: https://doi.org/10.1007/s00382-020-05620-9

[35] Ballarin, A.S., Sone, J.S., Gesualdo, G.C., et al, 2023. CLIMBra—Climate change dataset for Brazil. Scientific Data. 10, 47.
DOI: https://doi.org/10.1038/s41597-023-01956-z

[36] Cannon, A.J., Sobie, S.R., Murdock, T.Q., 2015. Bias correction of GCM precipitation by Quantile Mapping: How well do methods preserve changes in quantiles and extremes? Journal of Climate. 28, 6938–6959.
DOI: https://doi.org/10.1175/JCLI-D-14-00754.1

[37] Ferreira, G.W.S., Reboita, M.S., 2022. A new look into the South America precipitation regimes: Observation and forecast. Atmosphere. 13, 873.

DOI: https://doi.org/10.3390/atmos13060873

[38] Rupp, D.E., Abatzoglou, J.T., Hegewisch, K.C., et al., 2013. Evaluation of CMIP5 20th century climate simulations for the Pacific Northwest USA. Journal of Geophysical Research: Atmosphere. 118, 10884–10906.
DOI: https://doi.org/10.1002/jgrd.50843

[39] Ferreira, G.W.S., Reboita, M.S., Ribeiro, J.G.M., et al., 2023. Assessment of precipitation and hydrological droughts in South America through statistically downscaled CMIP6 projections. Climate. 11, 166.
DOI: https://doi.org/10.3390/cli11080166

[40] Ferreira, G.W.S., Reboita, M.S., Ribeiro, J.G.M., et al., 2024. Assessment of the wind power density over South America simulated by CMIP6 models in the present and future climate. Climate Dynamics. 62, 1729–1763.
DOI: https://doi.org/10.1007/s00382-023-06993-3

[41] Reboita, M.S., Ferreira, G.W.S., Ribeiro, J.G.M., et al., 2023. South American monsoon lifecycle projected by statistical downscaling with CMIP6-GCMs. Atmosphere. 14, 1380.
DOI: https://doi.org/10.3390/atmos14091380

[42] Reboita, M.S., Ferreira, G.W.S., Ribeiro, J.G.M., et al., 2024. Assessment of precipitation and near-surface temperature simulation by CMIP6 models in South America. Environmental Research: Climate. 3(2), 025001.
DOI: https://doi.org/10.1088/2752-5295/ad3fdb

[43] Dias, C.G., Reboita, M.S., 2021. Assessment of CMIP6 simulations over tropical South America. Revista Brasileira de Geografia Física. 14, 1282–1295.
DOI: https://doi.org/10.26848/rbgf.v14.3.p1282-1295

[44] Lovato, T., Peano, D., 2020. CMCC CMCC-CM2-SR5 model output prepared for CMIP6 CMIP historical Version 20200616. Earth System Grid Federation.
DOI: https://doi.org/10.22033/ESGF/CMIP6.3825

[45] Lovato, T., Peano, D., Butenschön, M., et al., 2022. CMIP6 simulations with the CMCC Earth System Model (CMCC-ESM2). Journal of Advances in Modeling Earth Systems. 14, e2021MS002814.
DOI: https://doi.org/10.1029/2021MS002814

[46] Döscher, R., Acosta, M., Alessandri, A., et al., 2022. The EC-Earth3 Earth System Model for the climate model intercomparison project 6. Geoscience Model Development. 15, 2973–3020.
DOI: https://doi.org/10.5194/gmd-15-2973-2022

[47] Krasting, J.P., John, J.G., Blanton, C.,et al., 2018. NOAA-GFDL GFDL-ESM4 model output prepared for CMIP6 CMIP historical. Version 20190726. Earth System Grid Federation.
DOI: https://doi.org/10.22033/ESGF/CMIP6.8597

[48] Boucher, O., Denvil, S., Levavasseur, G., et al., 2018. IPSL IPSL-CM6A-LR model output prepared for CMIP6 CMIP historical. Version 20180803. Earth System Grid Federation.
DOI: https://doi.org/10.22033/ESGF/CMIP6.5195

[49] Tatebe, H., Watanabe, M., 2018. MIROC MIROC6 model output prepared for CMIP6 CMIP historical. Version 20181212. Earth System Grid Federation.
DOI: https://doi.org/10.22033/ESGF/CMIP6.5603

[50] Wieners, K.H., Giorgetta, M., Jungclaus, J., et al., 2019, MPI-M MPI-ESM1.2-LR model output prepared for CMIP6 CMIP historical. Version 20190710. Earth System Grid Federation.
DOI: https://doi.org/10.22033/ESGF/CMIP6.6595

[51] Yukimoto, S., Koshiro, T., Kawai, H., et al., 2019. MRI MRI-ESM2.0 model output prepared for CMIP6 CMIP historical. Version 20190222. Earth System Grid Federation.
DOI: https://doi.org/10.22033/ESGF/CMIP6.6842

[52] Hersbach, H., Bell, B., Berrisford, P., et al., 2020. The ERA5 global reanalysis. Quarterly Journal of Royal Meteorological Society. 146, 1999–2049.
DOI: https://doi.org/10.1002/qj.3803

[53] Dullaart, J.C., Muis, S., Bloemendaal, N., et

al., 2020. Advancing global storm surge modelling using the new ERA5 climate reanalysis. Climate Dynamics. 54, 1007–1021.
DOI: https://doi.org/10.1007/s00382-019-05044-0

[54] Wilczak, J.M., Akish, E., Capotondi, A., et al., 2024. Evaluation and bias correction of the ERA5 reanalysis over the United States for wind and solar energy applications. Energies. 17, 1667.
DOI: https://doi.org/10.3390/en17071667

[55] Karlsson, K.-G., Stengel, M., Meirink, J.F., et al., 2023. CLARA-A3: The third edition of the AVHRR-based CM SAF climate data record on clouds, radiation and surface albedo covering the period 1979 to 2023. Earth System Science Data. 15, 4901–4926.
DOI: https://doi.org/10.5194/essd-15-4901-2023

[56] Boilley, A., Wald, L., 2015. Comparison between meteorological re-analyses from ERA-Interim and MERRA and measurements of daily solar irradiation at surface. Renewable Energy. 75, 135–143.
DOI: https://doi.org/10.1016/j.renene.2014.09.042

[57] Lee, T., Singh, V.P., 2018. Statistical downscaling for hydrological and environmental applications, 1st edition. CRC Press: Florida, USA. pp. 181.
DOI: https://doi.org/10.1201/9780429459580

[58] Tram-Anh, Q., Ngo-Duc, T., Espagne, E., et al., 2023. A 10-km CMIP6 downscaled dataset of temperature and precipitation for historical and future Vietnam climate. Scientific Data. 10, 257.
DOI: https://doi.org/10.1038/s41597-023-02159-2

[59] Climate change 2021: The Physical Science Basis [Internet] [cited 2024 Mar 10]. Available from: https://www.ipcc.ch/report/ar6/wg1/#FullReport

[60] Logan, T., Aoun, A., Bourgault, P., et al., 2022. Ouranosinc/xclim: v0.37.0 (v0.37.0). Zenodo.
DOI: https://doi.org/10.5281/zenodo.6671565

[61] Yilmaz, I.H., Mwesigye, A., 2018. Modeling, simulation and performance analysis of parabolic trough solar collectors: A comprehensive review. Applied Energy. 225, 135–174.
DOI: https://doi.org/10.1016/j.apenergy.2018.05.014

[62] Bellos, E., Tzivanidis, C., Tsimpoukis, D., 2018. Enhancing the performance of parabolic trough collectors using nanofluids and turbulators. Renewable and Sustainable Energy Reviews. 91, 358–375.
DOI: https://doi.org/10.1016/j.rser.2018.03.091

[63] He, Y., Yang, K., Wild, M., et al., 2023. Constrained future brightening of solar radiation and its implication for China's solar power. National Science Review. 10, nwac242.
DOI: https://doi.org/10.1093/nsr/nwac242

[64] Solar Thermal Electricity: Global Outlook 2016—Full Report [Internet] [cited 2024 Mar 25]. Available from: https://www.estelasolar.org/wp-content/uploads/2016/02/GP-ESTELA-SolarPACES_Solar-Thermal-Electricity-Global-Outlook-2016_Full-report.pdf

[65] Pereira, E.B., Martins, F.R., Gonçalves, A.R., et al., 2017. Brazilian solar energy atlas, 2nd Edition. (In Portuguese)
DOI: http://doi.org/10.34024/978851700089

[66] Renewable Energy Sources and Climate Change Mitigation—Special Report of the Intergovernmental Panel on Climate Change (IPCC) [Internet] [Accessed 2024 Mar 25]. Available from: https://www.ipcc.ch/report/renewable-energy-sources-and-climate-change-mitigation/

[67] Viviescas, C., Lima, L., Diuana, F.A., et al., 2019. Contribution of variable renewable energy to increase energy security in Latin America: Complementarity and climate change impacts on wind and solar resources. Renewable and Sustainable Energy Reviews. 113, 109232.
DOI: https://doi.org/10.1016/j.rser.2019.06.039

[68] Li, J., Huo, R., Chen, H., et al., 2021. Comparative assessment and future prediction using CMIP6 and CMIP5 for annual precipitation and extreme precipitation simulation. Frontiers

in Earth Science. 9, 2021.
DOI: https://doi.org/10.3389/feart.2021.687976

[69] Anderson, T., Duke, M., Morrison, G., et al., 2009. Performance of a building integrated photovoltaic/thermal (BIPVT) solar collector. Solar Energy. 83, 445–455.
DOI: https://doi.org/10.1016/j.solener.2008.08.013

[70] Trenberth, K.E., Fasullo, J., 2009. Global warming due to increasing absorbed solar radiation. Geophysical Research Letters. 36, L07706.
DOI: https://doi.org/10.1029/2009GL037527